1 **[231]Pa and [230]Th in the ocean model of the Community Earth System Model**
2 **(CESM1.3)**

3 Sifan Gu[1], Zhengyu Liu[1,2]

5 [1]Department of Atmospheric and Oceanic Sciences and Center for Climate Research,

6 University of Wisconsin-Madison, Madison, WI, USA

7 2. Now, affiliated with: Atmospheric Science Program, Department of Geography,

8 Ohio State University, Columbus, OH, USA

10 Correspondence to: Sifan Gu (sgu28@wisc.edu)

12 Abstract

13   Sediment ^{231}Pa/^{230}Th activity ratio is emerging as an important proxy for

14 deep ocean circulation in the past. In order to allow for a direct model-data

15 comparison and to improve our understanding of sediment ^{231}Pa/^{230}Th activity

16 ratio, we implement ^{231}Pa and ^{230}Th in the ocean component of the Community

17 Earth System Model (CESM). In addition to the fully coupled implementation of the

18 scavenging behavior of ^{231}Pa and ^{230}Th with the active marine ecosystem module (p-

19 coupled), another form of ^{231}Pa and ^{230}Th have also been implemented with

20 prescribed particle flux fields of the present climate (p-fixed). The comparison of the

21 two forms of ^{231}Pa and ^{230}Th helps to isolate the influence of the particle fluxes from

22 that of ocean circulation. Under present day climate forcing, our model is able to

23 simulate water column ^{231}Pa and ^{230}Th activity and sediment ^{231}Pa/^{230}Th activity

24 ratio in good agreement with available observations. In addition, the p-coupled and

25 p-fixed sediment ^{231}Pa/^{230}Th activity ratios behave similarly over large areas of low

26 productivity on long timescale to freshwater forcing, but can differ substantially in

27 some regions of high productivity and on short timescale, indicating the importance

28 of biological productivity in addition to ocean transport. Therefore, our model

29 provides a potentially powerful tool to help our interpretation of sediment

30 ^{231}Pa/^{230}Th reconstructions and to improve our understanding of past ocean

31 circulation and climate changes.

1. Introduction

Sediment ^{231}Pa/^{230}Th activity ratio has been used as a proxy for ocean circulation in the past (e.g. Yu et al. 1996; McManus et al. 2004; Gherardi et al. 2009). ^{231}Pa (32.5 ka half-life) and ^{230}Th (75.2 ka half-life) are produced at a constant rate approximately uniformly in the ocean by the α decay of ^{235}U and ^{234}U, respectively, with a production activity ratio of 0.093 (Henderson and Anderson, 2003). Water column ^{231}Pa and ^{230}Th are subject to particle scavenging and transport to sediments (Bacon and Anderson, 1982; Nozaki et al., 1987). Different scavenging efficiency results in different ocean residence time: ^{231}Pa has a residence time of approximately 111 years and ^{230}Th has a residence time of approximately 26 years (Yu et al., 1996). Longer residence time of ^{231}Pa than ^{230}Th makes ^{231}Pa more subject to ocean transport and therefore in the modern ocean about 45% of ^{231}Pa produced in the Atlantic is transported to the Southern Ocean (Yu et al., 1996), resulting a lower than 0.093 sediment ^{231}Pa/^{230}Th activity ratio in the North Atlantic and higher than 0.093 sediment ^{231}Pa/^{230}Th activity ratio in the Southern Ocean.

The application of the principle above to interpret sediment ^{231}Pa/^{230}Th as the strength of Atlantic meridional overturning circulation (AMOC), however, can be complicated by other factors, leading to uncertainties in using ^{231}Pa/^{230}Th as a proxy for past circulation (Keigwin and Boyle, 2008; Lippold et al., 2009; Scholten et al., 2008). In addition to the ocean transport, sediment ^{231}Pa/^{230}Th is also influenced by particle flux and composition (Chase et al., 2002; Geibert and Usbeck, 2004; Scholten et al., 2008; Siddall et al., 2007; Walter et al., 1997). The region of a higher particle flux tends to have a higher ^{231}Pa/^{230}Th (Kumar et al., 1993; Yong Lao et al., 1992), which is referred to as the "particle flux effect" (Siddall et al., 2005). Regional high particle flux in the water column will favor the removal of isotopes into the sediment, which leads to more isotopes transported into this region due to the down-gradient diffusive flux and subsequently more removal of isotopes into the sediment. Since ^{231}Pa has a longer residence time, this effect is more prominent on ^{231}Pa than on ^{230}Th and therefore sediment ^{231}Pa/^{230}Th will be higher in high productivity regions. Also, opal is able to scavenge ^{231}Pa much more effectively than ^{230}Th, leading to higher ^{231}Pa/^{230}Th in high opal flux regions such as the Southern

Ocean (Chase et al., 2002). Moreover, sediment ^{231}Pa/^{230}Th is suggested to record circulation change only within 1,000 m above the sediment, instead of the whole water column, complicating the interpretation of sediment ^{231}Pa/^{230}Th reconstructions (Thomas et al., 2006). For example, sediment ^{231}Pa/^{230}Th approaching 0.093 during Heinrich Stadial event 1(HS1) from the subtropical North Atlantic is interpreted as the collapse of AMOC (McManus et al., 2004). If sediment ^{231}Pa/^{230}Th only records deepest water mass, it is possible that during HS1, AMOC shoals, as opposed to a fully collapse, yet an increase of deep water imported from the Southern Ocean featuring high ^{231}Pa/^{230}Th can increase the sediment ^{231}Pa/^{230}Th approaching the production ratio (0.093) (Thomas et al., 2006). Therefore, it is important to incorporate ^{231}Pa and ^{230}Th into climate models for a direct model-data comparison and to promote a thorough understanding of sediment ^{231}Pa/^{230}Th as well as past ocean circulation.

^{231}Pa and ^{230}Th have been simulated in previous modeling studies (Dutay et al., 2009; Luo et al., 2010; Marchal et al., 2000; Rempfer et al., 2017; Siddall et al., 2005). Marchal et al., (2000) simulates ^{231}Pa and ^{230}Th in a zonally averaged circulation model, using the reversible scavenging model of Bacon and Anderson, (1982). One step further, Siddall et al. (2005) extends Marchal et al., (2000) by including particle dissolution with prescribed particle export production in a 3-D circulation model. Rempfer et al., (2017) further couples ^{231}Pa and ^{230}Th with active biogeochemical model and includes boundary scavenging and sediment resuspensions to improve model performance in simulating water column ^{231}Pa and ^{230}Th activity. Here we follow previous studies to implement ^{231}Pa and ^{230}Th into the Community Earth System Model (CESM). Our ^{231}Pa and ^{230}Th are coupled with active marine ecosystem model ("p-coupled") and p-coupled ^{231}Pa/^{230}Th is influenced by both ocean circulation change and particle flux change. To help to understand the influence of the particle flux, we have also implemented a "p-fixed" version of ^{231}Pa and ^{230}Th, for which the particle fluxes are fixed at prescribed values. Therefore, p-fixed ^{231}Pa/^{230}Th is only influenced by ocean circulation change. By comparing the p-fixed ^{231}Pa/^{230}Th with the p-coupled ^{231}Pa/^{230}Th, we will be able to separate the effect of circulation change from particle flux change. In

94 addition, the p-fixed ^{231}Pa and ^{230}Th can be run without the marine ecosystem
95 module, reducing computational cost by a factor of 3 in the ocean-alone model
96 simulation, making it a computationally efficient tracer for sensitivity studies.

97 This paper describes the details of ^{231}Pa and ^{230}Th in CESM and serves as a
98 reference for future studies using this tracer module. In section 2, we describe the
99 model and the implementation of ^{231}Pa and ^{230}Th. In sections 3, we describe the
100 experimental design. We will finally compare simulated ^{231}Pa and ^{230}Th fields with
101 observations, show model sensitivities on model parameter and also sediment
102 ^{231}Pa/^{230}Th ratio response to freshwater forcing in Section 4.

103

104 **2. Model Description**

105 2.1 Physical Ocean Model

106 We implement ^{231}Pa and ^{230}Th in the ocean model (Parallel Ocean Program
107 version 2, POP2) (Danabasoglu et al., 2012) of CESM (Hurrell et al., 2013). CESM is a
108 state-of-the-art coupled climate model and studies describing model components
109 and analyzing results can be found in a special collection in Journal of Climate
110 (http://journals.ametsoc.org/topic/ccsm4-cesm1). We run the ocean-alone model,
111 which is coupled to data atmosphere, land, ice and river runoff under the normal
112 year forcing of CORE-II data (Large and Yeager, 2008), using the low-resolution
113 version of POP2 with a nominal 3° horizontal resolution and 60 vertical layers.

114

115 2.2 Biogeochemical component (BGC)

116 CESM has incorporated a marine ecosystem module that simulates biological
117 variables (Moore et al., 2013). The marine ecosystem module has been validated
118 against present day observations extensively (e.g. Doney et al., 2009; Long et al.,
119 2013; Moore et al., 2002, 2004; Moore and Braucher, 2008). The implementation of
120 ^{231}Pa and ^{230}Th requires particle fields: $CaCO_3$, opal and particulate organic carbon
121 (POC). These particle fields can be obtained through the ecosystem driver from the
122 ecosystem module (Jahn et al., 2015). The ecosystem module simulates the particle
123 fluxes in reasonable agreement with the present-day observations. The pattern and
124 magnitude of the annual mean particle fluxes ($CaCO_3$, opal, POC) leaving the

125 euphotic zone at 105m are similar to the satellite observations (Fig. 7.2.5 and 9.2.2

126 in Sarmiento and Gruber 2006) (Fig. 1 a~c): particle fluxes are higher in the high

127 productivity regions such as high latitudes and equatorial Pacific; opal flux is high in

128 the Southern Ocean. The remineralization scheme of particle is based on the ballast

129 model of Armstrong et al., (2002). Detailed parameterizations for particle

130 remineralization are documented in Moore et al., (2004) with temperature

131 dependent remineralization length scales for POC and opal. We do not consider dust

132 because it is suggested to be unimportant for ^{231}Pa and ^{230}Th fractionation (Chase et

133 al., 2002; Siddall et al., 2005).

134

135 2.3 ^{231}Pa and ^{230}Th implementation

136   ^{231}Pa and ^{230}Th are produced from the α decay of ^{235}U and ^{234}U uniformly

137 everywhere at constant rate β^i (β^{Pa} = 2.33*10^{-3} dpm m^{-3} yr^{-1}, β^{Th} = 2.52*10^{-2} dpm m^{-3}

138 yr^{-1}). ^{231}Pa and ^{230}Th are also subjective to radioactive decay with the decay

139 constant of λ^i (λ^{Pa} = 2.13*10^{-5} yr^{-1}, λ^{Th} = 9.22*10^{-6} yr^{-1}).

140   Another important process contributes to ^{231}Pa and ^{230}Th activity is the

141 reversible scavenging by sinking particles (Bacon and Anderson, 1982), which

142 describes the adsorption of isotopes onto sinking particles and desorption after the

143 dissolution of particles. This process transports ^{231}Pa and ^{230}Th downward and

144 leads to a general increase of ^{231}Pa and ^{230}Th activity with depth. The reversible

145 scavenging considers total isotope activity (A_t^i) as two categories (Eq. (1)):

146 dissolved isotopes (A_d^i) and particulate isotopes (A_p^i) (superscript i refers to ^{231}Pa

147 and ^{230}Th) and A_p^i is the sum of the isotopes associated with different particle types

148 ($A_{j,p}^i$) (subscript j refers to different particle types: CaCO$_3$, opal and POC):

$$A_t^i = A_d^i + A_p^i = A_d^i + \sum_j A_{j,p}^i$$

149                                  (1)

150

151 Dissolved and particulate isotopes are assumed to be in equilibrium, which is a

152 reasonable assumption in the open ocean (Bacon and Anderson, 1982; Henderson et

al., 1999; Moore and Hunter, 1985). The ratio between the particulate isotope activity and the dissolved isotope activity is set by a partition coefficient, K (Eq. (2)):

$$K_j^i = \frac{A_{j,p}^i}{A_d^i \cdot R_j}$$ (2)

, where R_j is the ratio of particle concentration (C_j) to the density of seawater (1024.5 kg m^{-3}). Subscript j refers to different particle types (CaCO$_3$, opal and POC). Values of partition coefficient K used in our control simulation follows Chase et al., 2002 and Siddall et al., 2005 (Table 2).

Particulate isotopes (A_p^i) will be transported by sinking particles, which is described by $w_s \frac{\partial A_p^i}{\partial z}$ (Eq. (3)), where w_s is the sinking velocity. We don't differentiate between slow sinking small particles and rapid sinking large particles as in Dutay et al., (2009) and consider all particles as slowly sinking small particles with sinking velocity of w_s =1000 m yr^{-1} (Arsouze et al., 2009; Dutay et al., 2009; Kriest, 2002), which is similar to Rempfer et al., (2017) and Siddall et al., (2005). Any particulate isotopes (A_p^i) at the ocean bottom layer are removed from the ocean as sediment, which is the sink for the isotope budget. Detailed vertical differentiation scheme to calculate this term in the model is provided in the supplementary material. The reversible scavenging scheme applied here is the same as the neodymium implementation in POP2 (Gu et al., 2017).

Therefore, the conservation equation for ^{231}Pa and ^{230}Th activity can be written as

$$\frac{\partial A_t^i}{\partial t} = \beta^i - \lambda^i A_t^i - w_s \frac{\partial A_p^i}{\partial z} + Transport$$ (3),

where the total isotope activity is controlled by decay from U (first term), radioactive decay (second term), reversible scavenging (third term) and physical transport by the ocean model (fourth term, including advection, convection and diffusion). A_p^i can be calculated by combining Eq. (1) and Eq. (2):

180 $$A_t^i = A_d^i + A_d^i \cdot (K_{POC}^i \cdot R_{POC} + K_{CaCO_3}^i \cdot R_{CaCO_3} + K_{opal}^i \cdot R_{opal})$$

181 $$= A_d^i \cdot (1 + K_{POC}^i \cdot R_{POC} + K_{CaCO_3}^i \cdot R_{CaCO_3} + K_{opal}^i \cdot R_{opal}), \qquad (4)$$

182 which leads to

183 $$A_d^i = \frac{A_t^i}{1 + K_{POC}^i \cdot R_{POC} + K_{CaCO_3}^i \cdot R_{CaCO_3} + K_{opal}^i \cdot R_{opal}}, \qquad (5)$$

184 put this back to Eq. (1), we get

185 $$A_p^i = A_t^i \cdot (1 - \frac{1}{1 + K_{POC}^i \cdot R_{POC} + K_{CaCO_3}^i \cdot R_{CaCO_3} + K_{opal}^i \cdot R_{opal}}) \qquad (6)$$

186

187   Particle fields used in the reversible scavenging can be either prescribed or

188 simultaneously generated from the marine ecosystem module. Therefore, two forms

189 of [231]Pa and [230]Th are implemented in POP2: "p-fixed" and "p-coupled". P-fixed [231]Pa

190 and [230]Th use particle fluxes prescribed as annual mean particle fluxes generated

191 from the marine ecosystem module under present day climate forcing (Fig.1). P-

192 coupled [231]Pa and [230]Th use particle fluxes computed simultaneously from the

193 marine ecosystem module. P-fixed and p-coupled [231]Pa and [230]Th can be turned on

194 at the case build time and the p-coupled [231]Pa and [230]Th requires the ecosystem

195 module to be turned on at the same time.

196

197   Comparing with previous studies of modeling [231]Pa and [230]Th, our p-fixed

198 version is the same as Siddall et al., (2002), except that different prescribed particle

199 fluxes are used. The p-coupled version allows coupling to biogeochemical module,

200 which is similar to Rempfer et al., (2017), but we do not include boundary

201 scavenging and sediment resuspensions as in Rempfer et al., (2017) because

202 boundary scavenging and sediment resuspensions are suggested to be unimportant

203 to influence the relationship between [231]Pa$_p$/[230]Th$_p$ and AMOC strength (Rempfer et

204 al., 2017).

205

206 **3. Experiments**

207   We run a control experiment (CTRL) and two experiments with different

208   partition coefficients to show model sensitivity. We have both p-fixed and p-coupled

209   ^{231}Pa and ^{230}Th in CTRL, but only p-fixed ^{231}Pa and ^{230}Th in sensitivity experiments.

210   Equilibrium partition coefficients for ^{231}Pa and ^{230}Th vary among different particle

211   types and the magnitude of the partition coefficients for different particle types

212   remains uncertain (Chase et al., 2002; Chase and Robert F, 2004; Luo and Ku, 1999).

213   Since the control experiment in Siddall et al., (2005) is able to simulate major

214   features of ^{231}Pa and ^{230}Th distributions, we use the partition coefficients from the

215   control experiment in Siddall et al., (2005) in our CTRL (Table 2). Two sensitivity

216   experiments are performed with decreased (EXP_1) and increased (EXP_2) partition

217   coefficients by a factor of 5 (Table 2).

218   All the experiments are ocean-alone experiments with the normal year

219   forcing by CORE-II data (Large and Yeager, 2008). The ^{231}Pa and ^{230}Th activities are

220   initiated from 0 in CTRL and are integrated for 2,000 model years until equilibrium

221   is reached. EXP_1 and EXP_2 are initiated from 1,400 model year in CTRL and are

222   integrated for another 800 model years to reach equilibrium.

223   Since sediment ^{231}Pa/^{230}Th in North Atlantic has been used to reflect the

224   strength of AMOC, to test how sediment ^{231}Pa/^{230}Th in our model responds to the

225   change of AMOC and the change of particle fluxes, we carried out a fresh water

226   perturbation experiment (HOSING) with both p-fixed and p-coupled ^{231}Pa and ^{230}Th.

227   Starting from 2,000 model year of CTRL, a freshwater flux of 1 Sv is imposed over

228   the North Atlantic region of 50°N~70°N and the experiment is integrated for 1400

229   model years until both p-fixed and p-coupled sediment ^{231}Pa/^{230}Th ratio have

230   reached quasi-equilibrium. The partition coefficients used in HOSING are the same

231   as in CTRL.

232

233   **4. Results**

234   4.1 Control Experiment

235   P-fixed and p-coupled version of ^{231}Pa and ^{230}Th in CTRL show identical

236   results (Fig. 2-4). P-fixed and p-coupled dissolved and particulate ^{231}Pa and ^{230}Th in

237   CTRL are highly correlated with each other with correlations greater than 0.995 and

238   regression coefficients are all near 1.0 ($R^2 > 0.995$). The correlation coefficient

239   between p-fixed and p-coupled sediment $^{231}Pa/^{230}Th$ activity ratios in CTRL is 0.99

240   and the regression coefficient is 0.9 ($R^2 = 0.98$). This is expected because the particle

241   fields used in p-fixed version are prescribed as the climatology of the particle fields

242   used in the p-coupled version. Therefore, under the same climate forcing, p-fixed

243   and p-coupled version of ^{231}Pa and ^{230}Th should be very similar. For the discussion

244   of results in CTRL below, we only discuss the p-fixed ^{231}Pa and ^{230}Th.

245   The residence time of both ^{231}Pa and ^{230}Th in CTRL are comparable with

246   observations. The residence time is calculated as the ratio of global average total

247   isotope activity and the radioactive ingrowth of the isotope. Residence time in CTRL

248   is 118 yr for ^{231}Pa and 33 yr for ^{230}Th (Table 2), which are of the same magnitude as

249   111 yr for ^{231}Pa and 26 yr for ^{230}Th in observation (Yu et al., 1996).

250   CTRL can simulate the general features of dissolved water column ^{231}Pa and

251   ^{230}Th activities. Dissolved ^{231}Pa and ^{230}Th activities increase with depth in CTRL, as

252   shown in two GEOTRACES transects (Deng et al., 2014; Hayes et al., 2015) in the

253   Atlantic (Fig. 2 and 3). The dissolved ^{231}Pa and ^{230}Th activities in CTRL are also at

254   the same order of magnitude as in observations in the most of the ocean, except that

255   simulated values are larger than observations in the abyssal, which is also the case

256   in Siddall et al., (2005) and Rempfer et al., (2017) (their Fig. 2 and 3, experiment

257   Re3d). Our model is unable to simulate the realistic dissolved ^{231}Pa and ^{230}Th

258   activities in abyssal because boundary scavenging and sediment resuspensions are

259   not included in our model. With boundary scavenging and sediment resuspensions

260   added, dissolved ^{231}Pa and ^{230}Th activities in the abyssal should be greatly reduced

261   (Rempfer et al., 2017).

262   A more quantitative model-data comparison is shown in Fig. 5. The linear

263   regression coefficient between model results and observations (references of

264   observations are listed in Table 3), an indication of model ability to simulate ^{231}Pa

265   and ^{230}Th activity (Dutay et al., 2009), is near 1.0 for dissolved ^{231}Pa and ^{230}Th (1.02

266   for $[^{231}Pa]_d$ and 1.14 for $[^{230}Th]_d$), suggesting that CTRL can simulate the dissolved

267   ^{231}Pa and ^{230}Th in good agreement with observations. However, the simulation of

268   the particulate activity is not as good as the dissolved activity. Particulate activity is

269   overall larger than observation in the surface ocean and smaller than observation in

270   the deep ocean for both particulate [231]Pa and [230]Th. The regression coefficient for

271   particulate [231]Pa and [230]Th is 0.02 for $[^{231}Pa]_p$ and 0.05 for $[^{230}Th]_p$. The poor

272   performance in simulating water column particulate [231]Pa and [230]Th activities is also

273   in previous modeling studies (Dutay et al., 2009; Siddall et al., 2005), because of

274   similar modelling scheme are applied. However, the simulated $^{231}Pa_p/^{230}Th_p$ is in

275   reasonable agreement with observations. The $^{231}Pa_p/^{230}Th_p$ along two GEOTRACES

276   transects (Fig. 2 and 3) show the similar pattern and magnitude as in Rempfer et al.,

277   (2017), consistent with observations. Decrease of $^{231}Pa_p/^{230}Th_p$ with depth is well

278   simulated, which is suggested to be caused by the lateral transport of [231]Pa from

279   North Atlantic to Southern Ocean by AMOC (Gherardi et al., 2009; Lippold et al.,

280   2011, 2012a; Luo et al., 2010; Rempfer et al., 2017).

281   The sediment $^{231}Pa/^{230}Th$ in CTRL is overall consistent with observations

282   (references of observations are listed in Table 3). The North Atlantic shows low

283   sediment $^{231}Pa/^{230}Th$ activity ratio as in observations because [231]Pa is more subject

284   to the southward transport by active ocean circulation than [230]Th because of its

285   longer residence time. The Southern Ocean maximum in the sediment $^{231}Pa/^{230}Th$

286   activity ratio is also simulated in CTRL. High opal fluxes in the Southern Ocean,

287   which preferentially removes [231]Pa into sediment ($K_{opal}^{231Pa} > K_{opal}^{230Th}$) (Chase et al.,

288   2002), leading to increased sediment $^{231}Pa/^{230}Th$ activity ratio. In addition,

289   upwelling in the Southern Ocean brings up deep water enriched with [231]Pa, which is

290   transported from the North Atlantic, to shallower depth and further contribute to

291   the scavenging. CTRL can also produce higher sediment $^{231}Pa/^{230}Th$ activity ratio in

292   regions with high particle production (e.g. the Eastern equatorial Pacific, the North

293   Pacific and the Indian Ocean) due to the "particle flux effect". Specifically, in North

294   Atlantic, the distribution of sediment $^{231}Pa/^{230}Th$ matches the distribution of

295   particle, especially opal, production: sediment $^{231}Pa/^{230}Th$ is higher where opal

296   production is high, and vice versa (Fig. 4 and Fig. 1c).

297

298   4.2 Sensitivity on partition coefficient K

299   In this section, we show model sensitivity on partition coefficient by
300 increasing and decreasing the partition coefficient, K, by a factor of 5, but keep the
301 relative ratio for different particles the same (Table 2). Our model shows similar
302 model sensitivity as in Siddall et al., (2005) as discussed below.

303   As stated in Siddall et al., (2005), the isotope decay term in Eq. (3) is three
304 orders of magnitude less than the production term. If we neglect the transport term
305 and the decay term in Eq. (3) and assume particulate phase activity at the surface as
306 0, when reach equilibrium, the activity of particulate phase will be as in Eq. (7). Eq.
307 (7) combined with Eq.(2) and $R_i = \frac{F}{w_s * \rho}$, we can get Eq.(8). Under the assumption
308 that there is isotope decay and ocean transport, Eq. (7) suggests that the particulate
309 isotope activity depends on the production rate and settling velocity and will
310 increase linearly with depth. Eq. (8) suggests that the dissolved isotope activity
311 depends on the production rate, partition coefficient K and particle flux and will also
312 increase linearly with depth. Any departure from this linear relationship with depth
313 is due to ocean transport, which is suggested by observations (Bacon and Anderson,
314 1982; Roy-Barman et al., 1996). Results of Eq. (7) and Eq. (8) can help to understand
315 the differences in Exp_1 and Exp_2.

316   Increasing K will decrease water column dissolved ^{231}Pa and ^{230}Th activities
317 but won't change particulate ^{231}Pa and ^{230}Th too much (Fig. 6). Magnitude of
318 dissolved ^{231}Pa and ^{230}Th in Exp_1 (smaller K) is at least one order larger than that
319 in Exp_2 (larger K), while magnitude of particulate ^{231}Pa and ^{230}Th in Exp_1 and
320 Exp_2 is in the same order. As suggested by Eq. (8), if there is no isotope decay and
321 no ocean transport, larger K will lead to smaller dissolved isotope activity but
322 unchanged particulate activity. Intuitively, larger K will lead to more ^{231}Pa and ^{230}Th
323 attached to particles and further buried into sediment, which increases the sink for
324 the ^{231}Pa and ^{230}Th budget. With the sources for ^{231}Pa and ^{230}Th staying the same,
325 dissolved ^{231}Pa and ^{230}Th will be reduced. Increasing K will also reduce the vertical
326 gradient of dissolved ^{231}Pa and ^{230}Th as reversible scavenging act as the vertical
327 transport and increase this vertical transport can decrease the vertical gradient.
328 However, changes in the particulate ^{231}Pa and ^{230}Th is relatively small (Fig. 6). Eq.

329 (7) suggests that particulate phase activity it is independent of K. Therefore,
330 changing K will have limited influence on particulate phase activity.

331
$$A_p^i(z) = \frac{\beta^i}{w_s} \cdot z \qquad (7)$$

332
$$A_d^i(z) = \frac{\rho \beta^i}{K^i F} \cdot z \qquad (8)$$

333

334   Increasing K will also reduce the spatial gradient in sediment ^{231}Pa/^{230}Th
335 activity ratio and vice versa (Fig. 7). Larger K will decrease the ^{231}Pa and ^{230}Th
336 residence time and most isotopes produced in the water column are removed into
337 sediment locally (Table 2). Therefore, sediment ^{231}Pa/^{230}Th ratio becomes more
338 homogeneous and approaching the production ration of 0.093 (Fig. 7b). The
339 deviation (the root mean squared error) of sediment ^{231}Pa/^{230}Th is 0.0726 in CTRL,
340 0.0770 in Exp_1 and 0.0739 in Exp_2. Together with the water column isotope
341 activity, it suggests that the partition coefficient in CTRL is of the right order of
342 magnitude.

343

344 4.3. Sediment ^{231}Pa/^{230}Th ratio in HOSING

345   Potential changes in the export of biogenic particles makes using ^{231}Pa/^{230}Th
346 ratio to reconstructing AMOC strength under debate. In response to freshwater
347 perturbation in the North Atlantic, both biological productivity and AMOC strength
348 will change and will influence sediment ^{231}Pa/^{230}Th in different ways. Our model
349 with p-fixed and p-coupled ^{231}Pa and ^{230}Th can help to detangle these two effects. In
350 this section, we examine the sediment ^{231}Pa/^{230}Th (p-fixed and p-coupled) response
351 in the North Atlantic to idealized fresh water perturbation.

352   In HOSING, after applying freshwater forcing to the North Atlantic, AMOC
353 strength quickly decreases to a minimum of 2 Sv (AMOC_off) (Fig. 9a). During the
354 AMOC_off state, compared with CTRL with active AMOC (AMOC_on), p-fixed
355 sediment ^{231}Pa/^{230}Th shows an overall increase in the North Atlantic and a decrease
356 in the South Atlantic (Fig. 10b) because of the reduced southward transport of ^{231}Pa

357 from the North Atlantic by AMOC, consistent with paleo proxy evidence there (e.g.

358 Gherardi et al., 2005, 2009; McManus et al., 2004). The overall increase of sediment

359 ^{231}Pa/^{230}Th ratio in the North Atlantic in response to the AMOC collapse can be seen

360 more clearly in the time evolution of the sediment ^{231}Pa/^{230}Th ratio averaged from

361 20°N to 60°N in the North Atlantic (Fig.9b, green). Quantitatively, the ^{231}Pa/^{230}Th

362 increases from 0.074 in AMOC_on to 0.098 in AMOC_off in the p-fixed version,

363 approaching the production ration of 0.093. This increase of ^{231}Pa/^{230}Th is also in

364 the subtropical North Atlantic from the two sites near Bermuda Rise (Fig. 9e and f),

365 which is of comparable magnitude with the change from LGM to HS1 in

366 reconstructions there (McManus et al., 2004). In addition, the pattern of p-fixed

367 (Fig.10a) sediment ^{231}Pa/^{230}Th ratio during the Atlantic in AMOC_off state is similar

368 to the opal distribution (Fig.1b) because, without active circulation, sediment

369 ^{231}Pa/^{230}Th ratio is more controlled by particle flux effect, which is similar to the

370 Pacific in CTRL. It is further noted that our p-fixed sediment ^{231}Pa/^{230}Th ratio in

371 HOSING behaves similarly to that in Siddall et al., (2007).

372   The overall increase in p-fixed sediment ^{231}Pa/^{230}Th ratio in the North

373 Atlantic is not homogenous and the magnitude of the change between AMOC_on and

374 AMOC_off varies with location because of the distribution of particle flux, especially

375 opal flux (Fig.9 and 10). The maximum increase in p-fixed sediment ^{231}Pa/^{230}Th

376 ratio occurs near 40°N western Atlantic, where the opal production in our model is

377 maximum in North Atlantic (Fig. 1b). It should be noted that the opal maximum in

378 this region is not in the observation (Fig. 7.2.5 in Sarmiento and Gruber 2006).

379 However, our sediment ^{231}Pa/^{230}Th response in HOSING is self-consistent with the

380 particle flux in our model. The sediment ^{231}Pa/^{230}Th ratio in this region during

381 AMOC_on is larger than production ratio of 0.093 because opal maximum provides

382 extra ^{231}Pa to this region ("particle flux effect"), which overwhelms the active ocean

383 circulation transporting ^{231}Pa southward outside this region (Fig. 9d, green). During

384 AMOC_off, without active ocean circulation, the particle flux effect becomes even

385 stronger because less ^{231}Pa is transported out of the North Atlantic and p-fixed

386 sediment ^{231}Pa/^{230}Th ratio gets even larger.

387 In most regions of the Atlantic, p-coupled sediment ^{231}Pa/^{230}Th shows a
388 similar response to p-fixed ^{231}Pa/^{230}Th in HOSING. The evolution of p-fixed and p-
389 coupled sediment ^{231}Pa/^{230}Th activity ratio in HOSING are highly correlated (Fig.
390 11a). The change of sediment ^{231}Pa/^{230}Th ratio from AMOC_on to AMOC_off are
391 similar in both p-fixed and p-coupled version (Fig.11b). The correlation between p-
392 fixed and p-coupled sediment ^{231}Pa/^{230}Th ratio change from AMOC_on to AMOC_off
393 is 0.72 (1455points) and the linear regression coefficient is 0.71 (R^2 = 0.52). High
394 correlation between p-fixed and p-coupled response mainly happens over low
395 productivity regions (Fig.1, 10, and 11), where circulation effect on sediment
396 ^{231}Pa/^{230}Th is more important than the particle flux change in HOSING.

397 However, the responses of p-fixed and p-coupled sediment ^{231}Pa/^{230}Th to the
398 fresh water forcing can differ significantly in high productivity regions because of
399 the importance of the productivity change. With persistent freshwater forcing over
400 the North Atlantic, most regions in the North Atlantic show reduced production of
401 CaCO$_3$, opal and POC (Fig. 8). Productivity in the North Atlantic is suggested to be
402 halved during AMOC collapse because of increased stratification, which reduces
403 nutrient supply from deep ocean (Schmittner, 2005). In our model, the productivity
404 in the mid-latitude North Atlantic is indeed greatly reduced after the freshwater
405 forcing is applied. For example, opal production from 30°N-50°N in the Atlantic at
406 the end of HOSING is reduced by 50%~90% of its original value in CTRL. However,
407 opal production increases in high latitude North Atlantic (north of 50°N). The
408 pattern of opal production changes with high opal production region shifts
409 northward in HOSING (Fig. 8 d, e and f). These particle flux changes will influence
410 sediment ^{231}Pa/^{230}Th as discussed below.

411 North of 50°N in the Atlantic, the opal productivity increases during
412 AMOC_off (Fig. 8f) and will result an increase in sediment ^{231}Pa/^{230}Th. The increase
413 caused by greater opal productivity enhances the sediment ^{231}Pa/^{230}Th increase
414 caused by reduced AMOC. Therefore, the increase in p-coupled sediment ^{231}Pa/^{230}Th
415 from AMOC_on to AMOC_off is larger than p-fixed sediment ^{231}Pa/^{230}Th change
416 (Fig.9c).

417   In the mid-latitude North Atlantic, the opal productivity decreases during

418   AMOC_off (Fig.8 f) and will lead to a decrease in sediment ^{231}Pa/^{230}Th, which is

419   opposite to the effect of reduced AMOC. P-coupled sediment ^{231}Pa/^{230}Th shows an

420   initial decrease in first 200 years (Fig.9 d, e, and f, red dash lines) caused by the

421   reduced opal productivity. But this decrease trend is reversed eventually, suggesting

422   that the influence of particle flux change is overwhelmed by the effect of reduced

423   AMOC. It the long run, most regions in the subtropical and mid-latitude Atlantic

424   show increased sediment ^{231}Pa/^{230}Th in HOSING (Fig.10 d), indicating the dominant

425   effect of reduced AMOC. However, sediment ^{231}Pa/^{230}Th at 40°N west Atlantic,

426   where opal productivity is maximum during AMOC_on, show a decrease from

427   AMOC_on to AMOC_off (Fig.9 d and Fig.10 d). During AMOC_on, the opal productivity

428   maximum at 40°N west Atlantic lead to regional maximum sediment ^{231}Pa/^{230}Th

429   because of the particle flux effect (Fig. 4). During AMOC_off, this opal productivity

430   maximum is eliminated (Fig.8 e) and there is no more extra ^{231}Pa supplied by

431   surroundings to this region, which leads to a decrease in sediment ^{231}Pa/^{230}Th. This

432   decrease in sediment ^{231}Pa/^{230}Th caused by productivity change is greater than the

433   increase caused by the reduced AMOC. Therefore, sediment ^{231}Pa/^{230}Th experiences

434   a decrease from AMOC_on to AMOC_off at this location (Fig.9 d and Fig.10 d). Our

435   results suggest that although the circulation effect is more dominant than the

436   particle flux change in controlling sediment ^{231}Pa/^{230}Th on long time scale over

437   most of North Atlantic (Fig. 11), particle flux change can be important on short time

438   scale and in high productivity regions. With p-fixed and p-coupled ^{231}Pa and ^{230}Th,

439   our model can help to detangle the circulation effect and particle flux effect.

440

441   It is suggested that the particulate ^{231}Pa/^{230}Th response to the change of

442   AMOC depends on the location and depth. Above 2km and high latitude North

443   Atlantic, particulate ^{231}Pa/^{230}Th decreases with the increased AMOC (Rempfer et al.,

444   2017). Our results are consistent with this finding (Fig. 12 a and b). Both p-fixed and

445   p-coupled particulate ^{231}Pa/^{230}Th show similar patterns of change from AMOC_on to

446   AMOC_off: decrease in particulate ^{231}Pa/^{230}Th at shallow depth and north of 60°N

447   and increase in particulate ^{231}Pa/^{230}Th below 2km and south of 60°N during

448 AMOC_off. Therefore, sediment depth should also be taken into consideration when
449 interpreting sediment $^{231}Pa/^{230}Th$. Since the pattern in p-coupled is similar to the
450 pattern in p-fixed, the opposite particulate $^{231}Pa/^{230}Th$ changes in shallow and deep
451 North Atlantic is associated with AMOC change. During AMOC_on, upper limb of
452 AMOC (about upper 1km) transport water northward, which provides extra ^{231}Pa to
453 North Atlantic and particulate $^{231}Pa/^{230}Th$ is larger than the production ratio of
454 0.093. In contrast, the lower limb of AMOC (2km-3km) features southward
455 transport, which transports ^{231}Pa to the Southern Ocean and particulate $^{231}Pa/^{230}Th$
456 is smaller than the production ratio of 0.093 (Fig. 12 solid). Particulate $^{231}Pa/^{230}Th$
457 decreases with depth (Fig. 12 c solid). During AMOC_off, ocean transport of ^{231}Pa is
458 greatly reduced. Therefore, shallow (deep) depth experiences a decrease (increase)
459 in particulate $^{231}Pa/^{230}Th$ and the vertical gradient in the particulate $^{231}Pa/^{230}Th$ is
460 also greatly reduced (Fig. 12 c dash). Our results support that the depth dependence
461 of particulate $^{231}Pa/^{230}Th$ is mainly caused by lateral transport of ^{231}Pa by
462 circulation (Gherardi et al., 2009; Lippold et al., 2011, 2012a; Luo et al., 2010;
463 Rempfer et al., 2017).

464   Overall, our model is able to simulate the correct magnitude of the sediment
465 $^{231}Pa/^{230}Th$ ratio response to the freshwater forcing. Change of circulation has the
466 dominant influence on sediment $^{231}Pa/^{230}Th$ on long time scale over most of regions
467 in the idealized hosing experiment, although the detailed difference between p-fixed
468 and p-coupled sediment $^{231}Pa/^{230}Th$ ratio response to freshwater forcing in
469 different locations can be complicated.

470
471

472 **5. Summary**

473   ^{231}Pa and ^{230}Th have been implemented in the ocean model of the CESM in
474 both the p-coupled and p-fixed forms. Our control experiment under present day
475 climate forcing is able to simulate most ^{231}Pa and ^{230}Th water column activity and
476 sediment $^{231}Pa/^{230}Th$ activity ratio consistent with observations by using the
477 parameters that are suggested by Chase et al., (2002) and used in Siddall et al.

478 (2005). Our sensitivity experiments with varying parameters suggest that these
479 parameters are of the right order of magnitude.

480 Furthermore, our model is able to simulate the overall sediment ^{231}Pa/^{230}Th
481 ratio change in the North Atlantic with a magnitude comparable to the
482 reconstruction in response to the collapse of AMOC, although the detailed response
483 can be complicated in different regions. Finally, the p-fixed form is able to capture
484 many major features of that of the p-coupled form over large ocean areas on long
485 time scale, although the two forms can also differ significantly in some regions,
486 especially the region with high opal productivity.

487 However, our implementation of ^{231}Pa and ^{230}Th can be further improved by
488 including nepheloid layers to better simulate water column ^{231}Pa and ^{230}Th activity
489 as in Rempfer et al., 2017. In addition, partition coefficient for different particles can
490 be further tuned in the future, which can improve our understanding of the affinity
491 of ^{231}Pa and ^{230}Th to different particles, complementing the limited observational
492 studies available (e.g. Chase et al., 2002; Scholten et al., 2005; Walter et al., 1997).
493 Nevertheless, as the first attempt to implement ^{231}Pa and ^{230}Th in the CESM with
494 both p-fixed and p-coupled versions, our model can serve as a useful tool to improve
495 our understanding of the processes of ^{231}Pa and ^{230}Th and also interpretations of
496 sediment ^{231}Pa/^{230}Th reconstructions for past ocean circulation and climate
497 changes.

498
499

500 **Code availability:**
501 The ^{231}Pa and ^{230}Th isotope source code of both p-fixed and p-coupled versions for
502 CESM1.3 is included as supplementary material here.

503

504
505 **Acknowledgement:**
506 This work is supported by US NSF P2C2 program (NSF 1401778 and NSF1401802),
507), DOE DE-SC0006744 and the National Science Foundation of China No. 41630527
508 and 41130105. Computing resources (ark:/85065/d7wd3xhc) were provided by

509   the Climate Simulation Laboratory at NCAR's Computational and Information

510   Systems Laboratory, sponsored by the National Science Foundation and other

511   agencies.

512

513   **References:**

514   Anderson, R. F., Bacon, M. P. and Brewer, P. G.: Removal of230Th and231Pa from the
515   open ocean, Earth Planet. Sci. Lett., 62(1), 7–23, doi:10.1016/0012-821X(83)90067-
516   5, 1983.
517   Anderson, R. F., Lao, Y., Broecker, W. S., Trumbore, S. E., Hofmann, H. J. and Wolfli, W.:
518   Boundary scavenging in the Pacific Ocean: A comparison of 10Be and 231Pa, Earth
519   Planet. Sci. Lett., 96(3–4), 287–304, doi:10.1016/j.cognition.2008.05.007, 1990.
520   Anderson, R. F., Fleisher, M. Q., Biscaye, P. E., Kumar, N., Dittrich, B., Kubik, P. and
521   Suter, M.: Anomalous boundary scavenging in the Middle Atlantic Bight: evidence
522   from 230Th, 231Pa, 10Be and 210Pb, Deep. Res. Part II, 41(2–3), 537–561,
523   doi:10.1016/0967-0645(94)90034-5, 1994.
524   Armstrong, R. A., Lee, C., Hedges, J. I., Honjo, S. and Wakeham, S. G.: A new,
525   mechanistic model for organic carbon fluxes in the ocean based on the quantitative
526   association of POC with ballast minerals, Deep. Res. Part II Top. Stud. Oceanogr.,
527   49(1–3), 219–236, doi:10.1016/S0967-0645(01)00101-1, 2002.
528   Arsouze, T., Dutay, J.-C., Lacan, F. and Jeandel, C.: Reconstructing the Nd oceanic
529   cycle using a coupled dynamical – biogeochemical model, Biogeosciences, 6(12),
530   2829–2846, doi:10.5194/bg-6-2829-2009, 2009.
531   Bacon, M. and Anderson, R.: Distribution of Thorium Isotopes between dissolved
532   and particulate forms in the deep sea, J. Geophys. Res. …, 87(1), 2045–2056, 1982.
533   Bacon, M. P. and Rosholt, J. N.: Accumulation rates of 230Th, 231Pa, and some
534   transition metals on the Bermuda Rise, Geochim. Cosmochim. Acta, 46, 651–666,
535   1982.
536   Bacon, M. P., Huh, C. A. and Moore, R. M.: Vertical profiles of some natural
537   radionuclides over the Alpha Ridge, Arctic Ocean, Earth Planet. Sci. Lett., 95(1–2),
538   15–22, doi:10.1016/0012-821X(89)90164-7, 1989.
539   Bradtmiller, L. I., Anderson, R. F., Fleisher, M. Q. and Burckle, L. H.: Opal burial in the
540   equatorial Atlantic Ocean over the last 30 ka: Implications for glacial-interglacial
541   changes in the ocean silicon cycle, Paleoceanography, 22(4), 1–15,
542   doi:10.1029/2007PA001443, 2007.
543   Bradtmiller, L. I., McManus, J. F. and Robinson, L. F.: 231Pa/230Th evidence for a
544   weakened but persistent Atlantic meridional overturning circulation during
545   Heinrich Stadial 1, Nat. Commun., 5, 5817, doi:10.1038/ncomms6817, 2014.
546   Burckel, P., Waelbroeck, C., Luo, Y., Roche, D. M., Pichat, S., Jaccard, S. L., Gherardi, J.,
547   Govin, A., Lippold, J. and Thil, F.: Changes in the geometry and strength of the
548   Atlantic meridional overturning circulation during the last glacial (20-50 ka), Clim.
549   Past, 12(11), 2061–2075, doi:10.5194/cp-12-2061-2016, 2016.
550   Chase, Z. and Robert F, A.: Comment on "On the importance of opal, carbonate, and
551   lithogenic clays in scavenging and fractionating 230Th, 231Pa and 10Be in the ocean"

552   by S. Luo and T.-L. Ku, Earth Planet. Sci. Lett., 220(1–2), 201–211,

553   doi:10.1016/S0012-821X(04)00027-5, 2004.

554   Chase, Z., Anderson, R. F., Fleisher, M. Q. and Kubik, P. W.: The influence of particle

555   composition and particle flux on scavenging of Th , Pa and Be in the ocean, Earth

556   Planet. Sci. Lett., 204(1–2), 215–229, doi:10.1016/S0012-821X(02)00984-6, 2002.

557   Cochran, J. K., Livingston, H. D., Hirschberg, D. J. and Surprenant, L. D.: Natural and

558   anthropogenic radionuclide distributions in the northwest Atlantic Ocean, Earth

559   Planet. Sci. Lett., 84(2–3), 135–152, doi:10.1016/0012-821X(87)90081-1, 1987.

560   Cochran, J. K., Hirschberg, D. J., Livingston, H. D., Buesseler, K. O. and Key, R. M.:

561   Natural and anthropogenic radionuclide distributions in the Nansen Basin, Artic

562   Ocean: Scavenging rates and circulation timescales, Deep. Res. Part II, 42(6), 1495–

563   1517, doi:10.1016/0967-0645(95)00051-8, 1995.

564   Colley, S., Thomson, J. and Newton, P. P.: Detailed Th-230, Th-232 and Pb-210 fluxes

565   recorded by the 1989/90 BOFS sediment trap time-series at 48N, 20W, Deep - Sea

566   Res. Part I - Oceanogr. Res. Pap., 42(6), 833–848, 1995.

567   Coppola, L., Roy-Barman, M., Mulsow, S., Povinec, P. and Jeandel, C.: Thorium

568   isotopes as tracers of particles dynamics and deep water circulation in the Indian

569   sector of the Southern Ocean (ANTARES IV), Mar. Chem., 100(3–4 SPEC. ISS.), 299–

570   313, doi:10.1016/j.marchem.2005.10.019, 2006.

571   Danabasoglu, G., Bates, S. C., Briegleb, B. P., Jayne, S. R., Jochum, M., Large, W. G.,

572   Peacock, S. and Yeager, S. G.: The CCSM4 ocean component, J. Clim., 25(5), 1361–

573   1389, doi:10.1175/JCLI-D-11-00091.1, 2012.

574   DeMaster, D. J.: The marine budgets of silica and 32Si, Yale., 1979.

575   Deng, F., Thomas, A. L., Rijkenberg, M. J. A. and Henderson, G. M.: Controls on

576   seawater 231Pa, 230Th and 232Th concentrations along the flow paths of deep

577   waters in the Southwest Atlantic, Earth Planet. Sci. Lett., 390, 93–102,

578   doi:10.1016/j.epsl.2013.12.038, 2014.

579   Doney, S. C., Lima, I., Feely, R. A., Glover, D. M., Lindsay, K., Mahowald, N., Moore, J. K.

580   and Wanninkhof, R.: Mechanisms governing interannual variability in upper-ocean

581   inorganic carbon system and air-sea CO2 fluxes: Physical climate and atmospheric

582   dust, Deep. Res. Part II Top. Stud. Oceanogr., 56(8–10), 640–655,

583   doi:10.1016/j.dsr2.2008.12.006, 2009.

584   Dutay, J.-C., Lacan, F., Roy-Barman, M. and Bopp, L.: Influence of particle size and

585   type on 231 Pa and 230 Th simulation with a global coupled biogeochemical-ocean

586   general circulation model: A first approach, Geochemistry, Geophys. Geosystems,

587   10(1), doi:10.1029/2008GC002291, 2009.

588   Edmonds, H. N., Moran, S. B., Hoff, J. A., Smith, J. N. and Edwards, R. L.: Protactinium-

589   231 and Thorium-230 Abundances and High Scavenging Rates in the Western Arctic

590   Ocean, Science (80-.)., 280(5362), 405–407, doi:10.1126/science.280.5362.405,

591   1998.

592   Edmonds, H. N., Moran, S. B., Cheng, H. and Edwards, R. L.: 230Th and 231Pa in the

593   Arctic Ocean: Implications for particle fluxes and basin-scale Th/Pa fractionation,

594   Earth Planet. Sci. Lett., 227(1–2), 155–167, doi:10.1016/j.epsl.2004.08.008, 2004.

595   Francois, R., Bacon, M. P., Altabet, M. A. and Labeyrie, L. D.: Glacial/interglacial

596   changes in sediment rain rate in the SW Indian Sector of subantarctic Waters as

597   recorded by 230Th, 231Pa, U, and d15N, Paleoceanography, 8(5), 611–629,

598   doi:10.1029/93PA00784, 1993.

599   Frank, M.: Reconstruction of Late Quaternary environmental conditions applying the

600   natural radionuclides 230Th, 10Be, 231Pa and 238U: A study of deep-sea sediments

601   from the eastern sector of the Antarctic Circumpolar Current System, Alfred

602   Wegener Institute for Polar and Marine Research., 1996.

603   Frank, M., Eisenhauer, A., Kubik, P. W., Dittrich-hannen, B. and Segl, M.: Beryllium 10,

604   thorium 230, and protactinium 231 in Galapagos microplate sediments:

605   Implications of hydrothermal activity and paleoproductivity changes during the last

606   100,000 years, Palaeogeography, 9(4), 559–578, 1994.

607   Geibert, W. and Usbeck, R.: Adsorption of thorium and protactinium onto different

608   particle types: Experimental findings, Geochim. Cosmochim. Acta, 68(7), 1489–1501,

609   doi:10.1016/j.gca.2003.10.011, 2004.

610   Gherardi, J., Labeyrie, L., Mcmanus, J., Francois, R., Skinner, L. and Cortijo, E.:

611   Evidence from the Northeastern Atlantic basin for variability in the rate of the

612   meridional overturning circulation through the last deglaciation, Earth Planet. Sci.

613   Lett., 240(3–4), 710–723, doi:10.1016/j.epsl.2005.09.061, 2005.

614   Gherardi, J.-M., Labeyrie, L., Nave, S., Francois, R., McManus, J. F. and Cortijo, E.:

615   Glacial-interglacial circulation changes inferred from 231 Pa/ 230 Th sedimentary

616   record in the North Atlantic region, Paleoceanography, 24(2),

617   doi:10.1029/2008PA001696, 2009.

618   Gu, S., Liu, Z., Zhang, J., Rempfer, J., Joos, J., Brady, E. and Oppo, D.: Coherent response

619   of Antarctic Intermediate Water and Atlantic Meridional Overturning Circulation

620   during the last deglaciation, Palaeogeography, doi:10.1002/2017PA003092, 2017.

621   Guo, L., Santschi, P. H., Baskaran, M. and Zindler, A.: Distribution of dissolved and

622   particulate 230Th and 232Th in seawater from the Gulf of Mexico and off Cape

623   Hatteras as measured by SIMS, Earth Planet. Sci. Lett., 133(1), 117–128, 1995.

624   Gutjahr, M., Frank, M., Stirling, C. H., Keigwin, L. D. and Halliday, a. N.: Tracing the Nd

625   isotope evolution of North Atlantic Deep and Intermediate Waters in the western

626   North Atlantic since the Last Glacial Maximum from Blake Ridge sediments, Earth

627   Planet. Sci. Lett., 266(1–2), 61–77, doi:10.1016/j.epsl.2007.10.037, 2008.

628   Hall, I. R., Moran, S. B., Zahn, R., Knutz, P. C., Shen, C.-C. and Edwards, R. L.:

629   Accelerated drawdown of meridional overturning in the late-glacial Atlantic

630   triggered by transient pre-H event freshwater perturbation, Geophys. Res. Lett.,

631   33(16), L16616, doi:10.1029/2006GL026239, 2006.

632   Hayes, C. T., Anderson, R. F., Fleisher, M. Q., Serno, S., Winckler, G. and Gersonde, R.:

633   Quantifying lithogenic inputs to the North Pacific Ocean using the long-lived

634   thorium isotopes, Earth Planet. Sci. Lett., 383, 16–25,

635   doi:10.1016/j.epsl.2013.09.025, 2013.

636   Hayes, C. T., Anderson, R. F., Fleisher, M. Q., Huang, K. F., Robinson, L. F., Lu, Y., Cheng,

637   H., Edwards, R. L. and Moran, S. B.: [230]Th and [231]Pa on GEOTRACES GA03, the U.S.

638   GEOTRACES North Atlantic transect, and implications for modern and

639   paleoceanographic chemical fluxes, Deep. Res. Part II Top. Stud. Oceanogr., 116, 29–

640   41, doi:10.1016/j.dsr2.2014.07.007, 2015.

641   Henderson, G. M. and Anderson, R. F.: The U-series toolbox for paleoceanography,

642   Rev. Mineral. Geochemistry, 52(1), 493–531, doi:10.2113/0520493, 2003.

643   Henderson, G. M., Heinze, C., Anderson, R. F. and Winguth, A. M. E.: Global

644   distribution of the 230Th flux to ocean sediments constrained by GCM modelling,
645   Deep. Res. Part I Oceanogr. Res. Pap., 46(11), 1861–1893, doi:10.1016/S0967-
646   0637(99)00030-8, 1999.
647   Hoffmann, S. S., McManus, J. F., Curry, W. B. and Brown-Leger, L. S.: Persistent export
648   of 231Pa from the deep central Arctic Ocean over the past 35,000 years., Nature,
649   497(7451), 603–6, doi:10.1038/nature12145, 2013.
650   Hsieh, Y. Te, Henderson, G. M. and Thomas, A. L.: Combining seawater 232Th and
651   230Th concentrations to determine dust fluxes to the surface ocean, Earth Planet.
652   Sci. Lett., 312(3–4), 280–290, doi:10.1016/j.epsl.2011.10.022, 2011.
653   Huh, C. A. and Beasley, T. M.: Profiles of dissolved and particulate thorium isotopes
654   in the water column of coastal Southern California, Earth Planet. Sci. Lett., 85(1–3),
655   1–10, doi:10.1016/0012-821X(87)90016-1, 1987.
656   Hurrell, J. W., Holland, M. M., Gent, P. R., Ghan, S., Kay, J. E., Kushner, P. J., Lamarque, J.
657   F., Large, W. G., Lawrence, D., Lindsay, K., Lipscomb, W. H., Long, M. C., Mahowald, N.,
658   Marsh, D. R., Neale, R. B., Rasch, P., Vavrus, S., Vertenstein, M., Bader, D., Collins, W. D.,
659   Hack, J. J., Kiehl, J. and Marshall, S.: The community earth system model: A
660   framework for collaborative research, Bull. Am. Meteorol. Soc., 94(9), 1339–1360,
661   doi:10.1175/BAMS-D-12-00121.1, 2013.
662   Jahn, A., Lindsay, K., Giraud, X., Gruber, N., Otto-Bliesner, B. L., Liu, Z. and Brady, E. C.:
663   Carbon isotopes in the ocean model of the Community Earth System Model (CESM1),
664   Geosci. Model Dev., 8(8), 2419–2434, doi:10.5194/gmd-8-2419-2015, 2015.
665   Jonkers, L., Zahn, R., Thomas, A., Henderson, G., Abouchami, W., Fran??ois, R.,
666   Masque, P., Hall, I. R. and Bickert, T.: Deep circulation changes in the central South
667   Atlantic during the past 145 kyrs reflected in a combined 231Pa/230Th,
668   Neodymium isotope and benthic dC13 record, Earth Planet. Sci. Lett., 419, 14–21,
669   doi:10.1016/j.epsl.2015.03.004, 2015.
670   Keigwin, L. D. and Boyle, E. A.: Did North Atlantic overturning halt 17,000 years ago?,
671   Paleoceanography, 23(1), 1–5, doi:10.1029/2007PA001500, 2008.
672   Kriest, I.: Different parameterizations of marine snow in a 1D-model and their
673   influence on representation of marine snow, nitrogen budget and sedimentation,
674   Deep. Res. Part I Oceanogr. Res. Pap., 49(12), 2133–2162, doi:10.1016/S0967-
675   0637(02)00127-9, 2002.
676   Ku, T. L.: Uranium series disequilibrium in deep sea sediments, Columbia., 1966.
677   Ku, T. L., Bischoff, J. L. and Boersma, A.: Age studies of Mid-Atlantic Ridge sediments
678   near 42??N and 20??N, Deep. Res. Oceanogr. Abstr., 19(3), 233–247,
679   doi:10.1016/0011-7471(72)90033-2, 1972.
680   Kumar, N.: Trace metals and natural radionuclides as tracers of ocean productivity,
681   Columbia., 1994.
682   Kumar, N., Gwiazda, R., Anderson, R. F. and Froelich, P. N.: 231Pa/230Th ratios in
683   sediments as a proxy for past changes in Southern Ocean productivity, Nature, 362,
684   45–48, doi:10.1038/362045a0, 1993.
685   Large, W. G. and Yeager, S. G.: The global climatology of an interannually varying air–
686   sea flux data set, Clim. Dyn., 33(2–3), 341–364, doi:10.1007/s00382-008-0441-3,
687   2008.
688   Lippold, J., Grützner, J., Winter, D., Lahaye, Y., Mangini, A. and Christi, M.: Does
689   sedimentary 231Pa/230Th from the Bermuda Rise monitor past Atlantic Meridional

690   Overturning Circulation?, Geophys. Res. Lett., 36(12), 1–6,
691   doi:10.1029/2009GL038068, 2009.

692   Lippold, J., Gherardi, J. M. and Luo, Y.: Testing the [231]Pa/[230]Th paleocirculation proxy:
693   A data versus 2D model comparison, Geophys. Res. Lett., 38(20), 1–7,
694   doi:10.1029/2011GL049282, 2011.

695   Lippold, J., Mulitza, S., Mollenhauer, G., Weyer, S., Heslop, D. and Christl, M.:
696   Boundary scavenging at the East Atlantic margin does not negate use of 231Pa/
697   230Th to trace Atlantic overturning, Earth Planet. Sci. Lett., 333–334, 317–331,
698   doi:10.1016/j.epsl.2012.04.005, 2012a.

699   Lippold, J., Luo, Y., Francois, R., Allen, S. E., Gherardi, J., Pichat, S., Hickey, B. and
700   Schulz, H.: Strength and geometry of the glacial Atlantic Meridional Overturning
701   Circulation, Nat. Geosci., 5(11), 813–816, doi:10.1038/ngeo1608, 2012b.

702   Long, M. C., Lindsay, K., Peacock, S., Moore, J. K. and Doney, S. C.: Twentieth-century
703   oceanic carbon uptake and storage in CESM1(BGC), J. Clim., 26(18), 6775–6800,
704   doi:10.1175/JCLI-D-12-00184.s1, 2013.

705   Luo, S. and Ku, T. L.: Oceanic 231Pa/230Th ratio influenced by particle composition
706   and remineralization, Earth Planet. Sci. Lett., 167(3–4), 183–195,
707   doi:10.1016/S0012-821X(99)00035-7, 1999.

708   Luo, S. D., Ku, T. L., Kusakabe, M., Bishop, J. K. B. and Yang, Y. L.: Tracing particle
709   cycling in the upper ocean with Th-230 and Th-228: An investigation in the
710   equatorial Pacific along 140 degrees W, Deep - Sea Res. Part II - Top. Stud. Oceanogr.,
711   42(2–3), 805–829, doi:10.1016/0967-0645(95)00019-M, 1995.

712   Luo, Y., Francois, R. and Allen, S.: Sediment 231Pa/230Th as a recorder of the rate of
713   the Atlantic meridional overturning circulation: insights from a 2-D model, Ocean
714   Sci., 6(3), 381–400, doi:10.5194/os-6-381-2010, 2010.

715   Mangini, A. and Diester-Hass, L.: Excess Th-230 in sediments off NW Africa traces
716   upwelling during the past 130,000 years, in Coastal upwelling: Its sedimentary
717   records, edited by E. Suess and J. Thiede, pp. 455–470, Plenum., 1983.

718   Mangini, A. and Key, R. M.: A 230Th profile in the Atlantic Ocean, Earth Planet. Sci.
719   Lett., 62(3), 377–384, doi:10.1016/0012-821X(83)90008-0, 1983.

720   Mangini, A. and Sonntag, C.: 231Pa dating of deep-sea cores via 227Th counting,
721   Earth Planet. Sci. Lett., 37(2), 251–256, 1977.

722   Mangini, A. and U., K.: Depositional history in the Clarion-Clipperton zone during the
723   last 250,000 years: 230Th and 231Pa methods, Geol. Jahrb., 87, 105–121, 1987.

724   Marchal, O., François, R., Stocker, T. F. and Joos, F.: Ocean thermohaline circulation
725   and sedimentary 231Pa/230Th ratio, Paleoceanography, 15(6), 625–641 [online]
726   Available from: http://onlinelibrary.wiley.com/doi/10.1029/2000PA000496/full
727   (Accessed 19 April 2016), 2000.

728   McManus, J., Francois, R. and Gherardi, J.: Collapse and rapid resumption of Atlantic
729   meridional circulation linked to deglacial climate changes, Nature, 428(6985), 834–
730   837, 2004.

731   Moore, J. K. and Braucher, O.: Sedimentary and mineral dust sources of dissolved
732   iron to the World Ocean, Biogeosciences, 5(1994), 631–656, doi:10.5194/bgd-4-
733   1279-2007, 2008.

734   Moore, J. K., Doney, S. C., Glover, D. M. and Fung, I. Y.: Iron cycling and nutrient-
735   limitation patterns in surface waters of the World Ocean, , 49, 463–507, 2002.

736 Moore, J. K., Doney, S. C. and Lindsay, K.: Upper ocean ecosystem dynamics and iron
737 cycling in a global three-dimensional model, Global Biogeochem. Cycles, 18(4),
738 doi:10.1029/2004GB002220, 2004.
739 Moore, J. K., Lindsay, K., Doney, S. C., Long, M. C. and Misumi, K.: Marine Ecosystem
740 Dynamics and Biogeochemical Cycling in the Community Earth System Model
741 [CESM1(BGC)]: Comparison of the 1990s with the 2090s under the RCP4.5 and
742 RCP8.5 Scenarios, J. Clim., 26(23), 9291–9312, doi:10.1175/JCLI-D-12-00566.1,
743 2013.
744 Moore, R. M. and Hunter, K. A.: Thorium adsorption in the ocean: reversibility and
745 distribution amongst particle sizes, Geochim. Cosmochim. Acta, 49(11), 2253–2257,
746 doi:10.1016/0016-7037(85)90225-X, 1985.
747 Moore, W. S.: The thorium isotope content of ocean water, Earth Planet. Sci. Lett.,
748 53(3), 419–426, doi:10.1016/0012-821X(81)90046-7, 1981.
749 Moran, S. B., Hoff, J. A., Buesseler, K. O. and Edwards, R. L.: High precision 230Th and
750 232Th in the Norwegian Sea and Denmark by thermal ionization mass
751 spectrometry, , 22(19), 2589–2592, 1995.
752 Moran, S. B., Charette, M. a., Hoff, J. a., Edwards, R. L. and Landing, W. M.: Distribution
753 of 230Th in the Labrador Sea and its relation to ventilation, Earth Planet. Sci. Lett.,
754 150, 151–160, doi:10.1016/S0012-821X(97)00081-2, 1997.
755 Moran, S. B., Shen, C.-C., Weinstein, S. E., Hettinger, L. H., Hoff, J. H., E dmonds, H. N.
756 and Edwards, R. L.: Constraints on deep water age and particle flux in the Equatorial
757 and South Atlantic Ocean based on seawater 231Pa and 230Th data, Geophys. Res.
758 Lett., 28(18), 3437–3440 [online] Available from:
759 papers2://publication/uuid/2A811583-B32B-4BD8-B582-EC8B0D96A949, 2001.
760 Moran, S. B., Shen, C. C., Edmonds, H. N., Weinstein, S. E., Smith, J. N. and Edwards, R.
761 L.: Dissolved and particulate 231Pa and 230Th in the Atlantic Ocean: Constraints on
762 intermediate/deep water age, boundary scavenging, and 231Pa/230Th
763 fractionation, Earth Planet. Sci. Lett., 203(3–4), 999–1014, doi:10.1016/S0012-
764 821X(02)00928-7, 2002.
765 Müller, P. J. and Mangini, A.: Organic carbon decomposition rates in sediments of the
766 pacific manganese nodule belt dated by 230Th and 231Pa, Earth Planet. Sci. Lett.,
767 51(1), 94–114, doi:10.1016/0012-821X(80)90259-9, 1980.
768 Negre, C., Zahn, R., Thomas, A. L., Masqué, P., Henderson, G. M., Martínez-Méndez, G.,
769 Hall, I. R. and Mas, J. L.: Reversed flow of Atlantic deep water during the Last Glacial
770 Maximum., Nature, 468(7320), 84–88, doi:10.1038/nature09508, 2010.
771 Nozaki, Y. and Horibe, Y.: Alpha-emitting thorium isotopes in northwest Pacific deep
772 waters, Earth Planet. Sci. Lett., 65(1), 39–50, doi:10.1016/0012-821X(83)90188-7,
773 1983.
774 Nozaki, Y. and Nakanishi, T.: 231Pa and 230Th profiles in the open ocean water
775 column, Deep Sea Res. Part A, Oceanogr. Res. Pap., 32(10), 1209–1220,
776 doi:10.1016/0198-0149(85)90004-4, 1985.
777 Nozaki, Y. and Yamada, M.: Thorium and protactinium isotope distributions in
778 waters of the Japan Sea, Deep Sea Res. Part A, Oceanogr. Res. Pap., 34(8), 1417–1430,
779 1987.
780 Nozaki, Y. and Yang, H. S.: Th and Pa isotopes in the waters of the western margin of
781 the pacific near Japan: Evidence for release of228Ra and227Ac from slope

782 sediments, J. Oceanogr. Soc. Japan, 43(4), 217–227, doi:10.1007/BF02109817, 1987.

783 Nozaki, Y., Horibe, Y. and Tsubota, H.: The water column distribution of thorium
784 isotopes in the western North Pacific, Earth Planet. Sci. Lett., 54(54), 203–216, 1981.

785 Nozaki, Y., Yang, H.-S. and Yamada, M.: Scavenging of thorium in the ocean, J.
786 Geophys. Res., 92(C1), 772, doi:10.1029/JC092iC01p00772, 1987.

787 Okubo, A., Obata, H., Nozaki, Y., Yamamoto, Y. and Minami, H.: 230Th in the
788 Andaman Sea: Rapid deep-sea renewal, Geophys. Res. Lett., 31(22), 1–5,
789 doi:10.1029/2004GL020226, 2004.

790 Okubo, A., Obata, H., Luo, S., Gamo, T., Yamamoto, Y., Minami, H. and Yamada, M.:
791 Particle flux in the twilight zone of the eastern Indian Ocean: A constraint from
792 234U-230Th and 228Ra-228Th disequilibria, Deep. Res. Part I Oceanogr. Res. Pap.,
793 54(10), 1758–1772, doi:10.1016/j.dsr.2007.06.009, 2007a.

794 Okubo, A., Obata, H., Gamo, T., Minami, H. and Yamada, M.: Scavenging of 230Th in
795 the Sulu Sea, Deep. Res. Part II Top. Stud. Oceanogr., 54(1–2), 50–59,
796 doi:10.1016/j.dsr2.2006.02.016, 2007b.

797 Okubo, A., Obata, H., Gamo, T. and Yamada, M.: 230Th and 232Th distributions in
798 mid-latitudes of the North Pacific Ocean: Effect of bottom scavenging, Earth Planet.
799 Sci. Lett., 339–340, 139–150, doi:10.1016/j.epsl.2012.05.012, 2012.

800 Rempfer, J., Stocker, T. F., Joos, F., Lippold, J. and Jaccard, S. L.: New insights into
801 cycling of 231 Pa and 230 Th in the Atlantic Ocean, Earth Planet. Sci. Lett., 468, 27–
802 37, doi:10.1016/j.epsl.2017.03.027, 2017.

803 Roberts, N. L., McManus, J. F., Piotrowski, A. M. and McCave, I. N.: Advection and
804 scavenging controls of Pa/Th in the northern NE Atlantic, Paleoceanography, 29(6),
805 668–679, doi:10.1002/2014PA002633, 2014.

806 Robinson, L. F., Belshaw, N. S. and Henderson, G. M.: U and Th concentrations and
807 isotope ratios in modern carbonates and waters from the Bahamas, Geochim.
808 Cosmochim. Acta, 68(8), 1777–1789, doi:10.1016/j.gca.2003.10.005, 2004.

809 Roy-Barman, M., Chen, J. H. and Wasserburg, G. J.: 230Th-232Th systematics in the
810 central Pacific Ocean: The sources and the fates of thorium, Earth Planet. Sci. Lett.,
811 139(3–4), 351–363, doi:10.1016/0012-821X(96)00017-9, 1996.

812 Rutgers van der Loeff, M. M. and Berger, G. W.: Scavenging of 230Th and 231Pa near
813 the antarctic polar front in the South Atlantic, Deep. Res. Part I, 40(2), 339–357,
814 doi:10.1016/0967-0637(93)90007-P, 1993.

815 Schmittner, A.: Decline of the marine ecosystem caused by a reduction in the
816 Atlantic overturning circulation., Nature, 434(7033), 628–633,
817 doi:10.1038/nature03476, 2005.

818 Schmitz, W., Mangini, A., Stoffers, P., Glasby, G. P. and Pluger, W. L.: Sediment
819 accumulation rates in the southwestern Pacific Basin and Aitutaki Passage, Mar.
820 Geol., 73(1), 181–190, 1986.

821 Scholten, J. C., Rutgers van der Loeff, M. M. and Michel, A.: Distribution of 230Th and
822 231Pa in the water column in relation to the ventilation of the deep Arctic basins,
823 Deep. Res. Part II, 42(6), 1519–1531, doi:10.1016/0967-0645(95)00052-6, 1995.

824 Scholten, J. C., Fietzke, J., Mangini, A., Stoffers, P., Rixen, T., Gaye-Haake, B., Blanz, T.,
825 Ramaswamy, V., Sirocko, F., Schulz, H. and Ittekkot, V.: Radionuclide fluxes in the
826 Arabian Sea: The role of particle composition, Earth Planet. Sci. Lett., 230(3–4), 319–
827 337, doi:10.1016/j.epsl.2004.11.003, 2005.

828 Scholten, J. C., Fietzke, J., Mangini, A., Garbe-Schönberg, C. D., Eisenhauer, A.,
829 Schneider, R. and Stoffers, P.: Advection and scavenging: Effects on 230Th and
830 231Pa distribution off Southwest Africa, Earth Planet. Sci. Lett., 271(1–4), 159–169,
831 doi:10.1016/j.epsl.2008.03.060, 2008.
832 Shimmield, G. B. and Price, N. B.: The scavenging of U,230Th and 231Pa during
833 pulsed hydrothermal activity at 20??S, East Pacific Rise, Geochim. Cosmochim. Acta,
834 52(3), 669–677, doi:10.1016/0016-7037(88)90329-8, 1988.
835 Shimmield, G. B., Murray, J. W., Thomson, J., Bacon, M. P., Anderson, R. F. and Price, N.
836 B.: The distribution and behaviour of 230Th and 231Pa at an ocean margin, Baja
837 California, Mexico, Geochim. Cosmochim. Acta, 50(11), 2499–2507,
838 doi:10.1016/0016-7037(86)90032-3, 1986.
839 Siddall, M., Henderson, G. M., Edwards, N. R., Frank, M., Müller, S. a., Stocker, T. F. and
840 Joos, F.: 231Pa/230Th fractionation by ocean transport, biogenic particle flux and
841 particle type, Earth Planet. Sci. Lett., 237(1–2), 135–155,
842 doi:10.1016/j.epsl.2005.05.031, 2005.
843 Siddall, M., Stocker, T. F., Henderson, G. M., Joos, F., Frank, M., Edwards, N. R., Ritz, S.
844 P. and Müller, S. a.: Modeling the relationship between 231 Pa/ 230 Th distribution
845 in North Atlantic sediment and Atlantic meridional overturning circulation,
846 Paleoceanography, 22(2), n/a-n/a, doi:10.1029/2006PA001358, 2007.
847 Thomas, A. L., Henderson, G. M. and Robinson, L. F.: Interpretation of the
848 231Pa/230Th paleocirculation proxy: New water-column measurements from the
849 southwest Indian Ocean, Earth Planet. Sci. Lett., 241(3–4), 493–504,
850 doi:10.1016/j.epsl.2005.11.031, 2006.
851 Trimble, S. M., Baskaran, M. and Porcelli, D.: Scavenging of thorium isotopes in the
852 Canada Basin of the Arctic Ocean, Earth Planet. Sci. Lett., 222(3–4), 915–932,
853 doi:10.1016/j.epsl.2004.03.027, 2004.
854 Venchiarutti, C., van der Loeff, M. R. and Stimac, I.: Scavenging of 231Pa and thorium
855 isotopes based on dissolved and size-fractionated particulate distributions at Drake
856 Passage (ANTXXIV-3), Deep. Res. Part II Top. Stud. Oceanogr., 58(25–26), 2767–
857 2784, doi:10.1016/j.dsr2.2010.10.040, 2011.
858 Vogler, S., Scholten, J., Rutgers van der Loeff, M. M. and Mangini, A.: 230Th in the
859 eastern North Atlantic: the importance of water mass ventilation in the balance of
860 230Th, Earth Planet. Sci. Lett., 156(1–2), 61–74, doi:10.1016/S0012-
861 821X(98)00011-9, 1998.
862 Walter, H. J., Rutgers van der Loeff, M. M. and Hoeltzen, H.: Enhanced scavenging of
863 231Pa relative to 230Th in the South Atlantic south of the Polar Front: Implications
864 for the use of the 231Pa/230Th ratio as a paleoproductivity proxy, Earth Planet. Sci.
865 Lett., 149(1), 85–100, doi:10.1016/S0012-821X(97)00068-X, 1997.
866 Yang, H. S., Nozaki, Y., Sakai, H. and Masuda, A.: The distribution of 230Th and 231Pa
867 in the deep-sea surface sediments of the Pacific Ocean, Geochim. Cosmochim. Acta,
868 50(1), 81–89, doi:10.1016/0016-7037(86)90050-5, 1986.
869 Yong-Liang Yang, Elderfield, H., Pedersen, T. F. and Ivanovich, M.: Geochemical
870 record of the Panama Basin during the Last Glacial Maximum carbon event shows
871 that the glacial ocean was not suboxic, Geology, 23(12), 1115–1118,
872 doi:10.1130/0091-7613(1995)023<1115:GROTPB>2.3.CO, 1995.
873 Yong Lao, Anderson, R. F., Broecker, W. S., Trumbore, S. E., Hofmann, H. J. and Wolfli,

874   W.: Transport and burial rates of 10Be and 231Pa in the Pacific Ocean during the
875   Holocene period, Earth Planet. Sci. Lett., 113(1–2), 173–189, doi:10.1016/0012-
876   821X(92)90218-K, 1992.
877   Yu, E.-F.: Variations in the Particulate Flux of 230Th and 231Pa and
878   Paleoceanographic Applications of the 231Pa/230Th Ratio, WHOI/MIT., 1994.
879   Yu, E.-F., Francois, R. and Bacon, M. P.: Similar rates of modern and last-glacial ocean
880   thermohaline circulation inferred from radiochemical data, Nature, 379(6567),
881   689–694, doi:10.1038/379689a0, 1996.
882

Variable	Symbol	Value	Units
Production of ^{231}Pa from U decay	β^{Pa}	$2.33*10^{-3}$	dpm m^{-3} yr^{-1}
Production of ^{230}Th from U decay	β^{Th}	$2.52*10^{-2}$	dpm m^{-3} yr^{-1}
Decay constant of ^{231}Pa	λ^{Pa}	$2.13*10^{-5}$	yr^{-1}
Decay constant of ^{230}Th	λ^{Th}	$9.22*10^{-6}$	yr^{-1}
Index for ^{231}Pa and ^{230}Th	i		
Index for particle type	j		
Total isotope activity	A_t		dpm m^{-3}
Dissolved isotope activity	A_d		dpm m^{-3}
Particle associated activity	A_p		dpm m^{-3}
Particle settling velocity	w_s	1000	m yr^{-1}
Particle concentration	C		kg m^{-3}
Density of seawater		1024.5	kg m^{-3}
Ratio between particle concentration and density of seawater	R		

883 Table 1. List of parameters, abbreviations and values.
884
885

	CTRL		EXP_1		EXP_2	
	^{231}Pa	^{230}Th	^{231}Pa	^{230}Th	^{231}Pa	^{230}Th
K_{CaCO_3}	$2.5*10^5$	$1.0*10^7$	$5*10^4$	$2*10^6$	$1.25*10^6$	$5*10^7$
K_{opal}	$1.67*10^6$	$5*10^5$	$3.33*10^5$	$1*10^5$	$8.33*10^6$	$2.5*10^6$
K_{POC}	$1.0*10^7$	$1.0*10^7$	$2*10^6$	$2*10^6$	$5*10^7$	$5*10^7$
τ (yr)	118	33	501	143	27	9

886 Table 2. Partition coefficients for different particle types and residence time for
887 ^{231}Pa and ^{230}Th in different experiments. Partition coefficients used in CTRL follows
888 (Chase et al., 2002; Siddall et al., 2005). Both p-coupled and p-fixed versions are
889 enabled in CTRL, which yields identical results (discussed in section 4.1). Only p-
890 fixed version is enabled in Exp_1 and Exp_2. The residence time (τ) is for p-fixed
891 version in each experiment.
892

WATER COLUMN ACTIVITY	Holocene core-top ^{231}Pa/^{230}Th
(Guo et al., 1995)	(Yu, 1994)
(Cochran et al., 1987)	(DeMaster, 1979)
(Nozaki et al., 1987)	(Bacon and Rosholt, 1982)
(Bacon and Anderson, 1982)	(Mangini and Diester-Hass, 1983)
(Bacon et al., 1989)	(Kumar, 1994)

(Huh and Beasley, 1987)	(Yang et al., 1986)
(Rutgers van der Loeff and Berger, 1993)	(Anderson et al., 1983)
(Nozaki et al., 1981)	(Anderson et al., 1994)
(Nozaki and Nakanishi, 1985)	(Ku, 1966)
(Mangini and Key, 1983)	(Ku et al., 1972)
(Nozaki and Horibe, 1983)	(Frank et al., 1994)
(Moore, 1981)	(Shimmield et al., 1986)
(Nozaki and Yamada, 1987)	(Frank, 1996)
(Roy-Barman et al., 1996)	(Yong Lao et al., 1992)
(Nozaki and Yang, 1987)	(Francois et al., 1993)
(Moran et al., 1995)	(Anderson et al., 1990)
(Luo et al., 1995)	(Mangini and Sonntag, 1977)
(Colley et al., 1995)	(Schmitz et al., 1986)
(Scholten et al., 1995)	(Shimmield and Price, 1988)
(Cochran et al., 1995)	(Yong-Liang Yang et al., 1995)
(Vogler et al., 1998)	(Müller and Mangini, 1980)
(Moran et al., 1997)	(Mangini and U., 1987)
(Edmonds et al., 1998)	(Scholten et al., 1995)
(Moran et al., 2001)	(Walter et al., 1997)
(Edmonds et al., 2004)	(Lippold et al., 2011)
(Okubo et al., 2007b)	(Lippold et al., 2012b)
(Coppola et al., 2006)	(Bradtmiller et al., 2007)
(Moran et al., 2002)	(Gherardi et al., 2005)
(Okubo et al., 2004)	(Gutjahr et al., 2008)
(Okubo et al., 2007a)	(Hall et al., 2006)
(Okubo et al., 2012)	(Lippold et al., 2011)
(Robinson et al., 2004)	(Roberts et al., 2014)
(Thomas et al., 2006)	(Bradtmiller et al., 2014)
(Trimble et al., 2004)	(Burckel et al., 2016)
(Venchiarutti et al., 2011)	(Hoffmann et al., 2013)
(Hsieh et al., 2011)	(Jonkers et al., 2015)
(Scholten et al., 2008)	(Negre et al., 2010)
(Luo et al., 2010)	
(Deng et al., 2014)	
(Hayes et al., 2013)	
(Hayes et al., 2015)	

893
894
895   Table 3. References for observations of water column ^{231}Pa and ^{230}Th activity and
896   Holocene core-top ^{231}Pa/^{230}Th.
897

898

899

900

901

902

903

904

905

906

907

908

909

910

911

912

913

914

915

916

917

918

919   Figures:
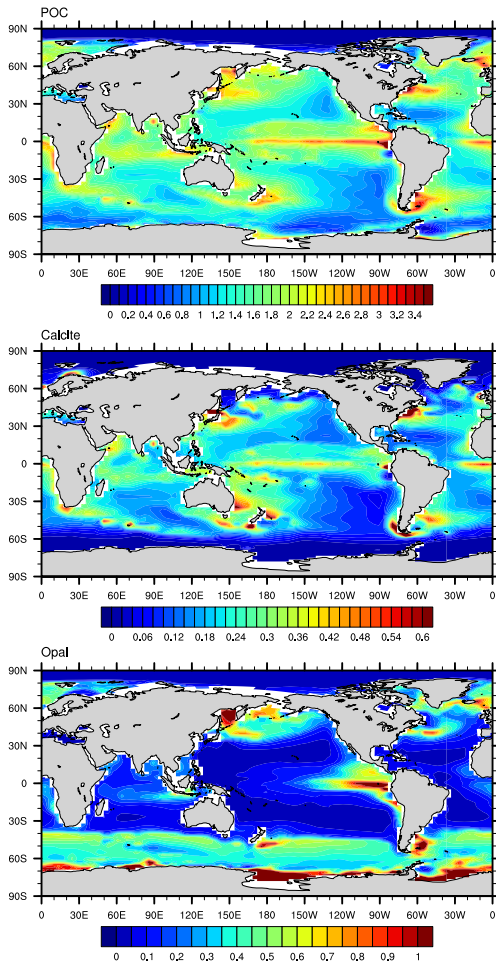
920

921   Figure 1. Annual mean particle fluxes in CESM. (a) $CaCO_3$ flux at 105m (mol m^{-2} yr^{-1}).

922   (b) Opal flux at 105m (mol m^{-2} yr^{-1}). (c) POC flux at 105m (mol m^{-2} yr^{-1}).

923

924

925
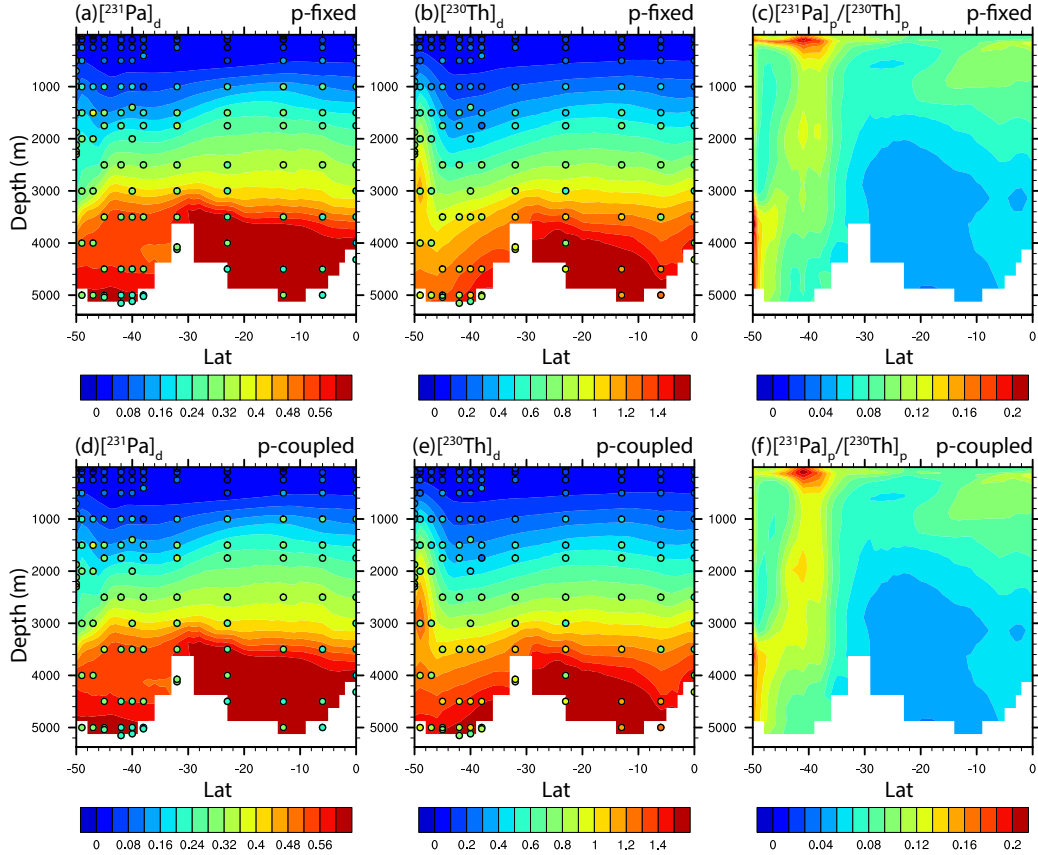
Figure 2. Dissolved ^{231}Pa, dissolved ^{230}Th and particulate ^{231}Pa/^{230}Th in CTRL along GEOTRACES transect GA02S (Deng et al., 2014) (the track is indicated in Fig. S4) for both p-fixed and p-coupled ^{231}Pa and ^{230}Th. Observations of dissolved ^{231}Pa and ^{230}Th activity are superimposed using the same colormap.
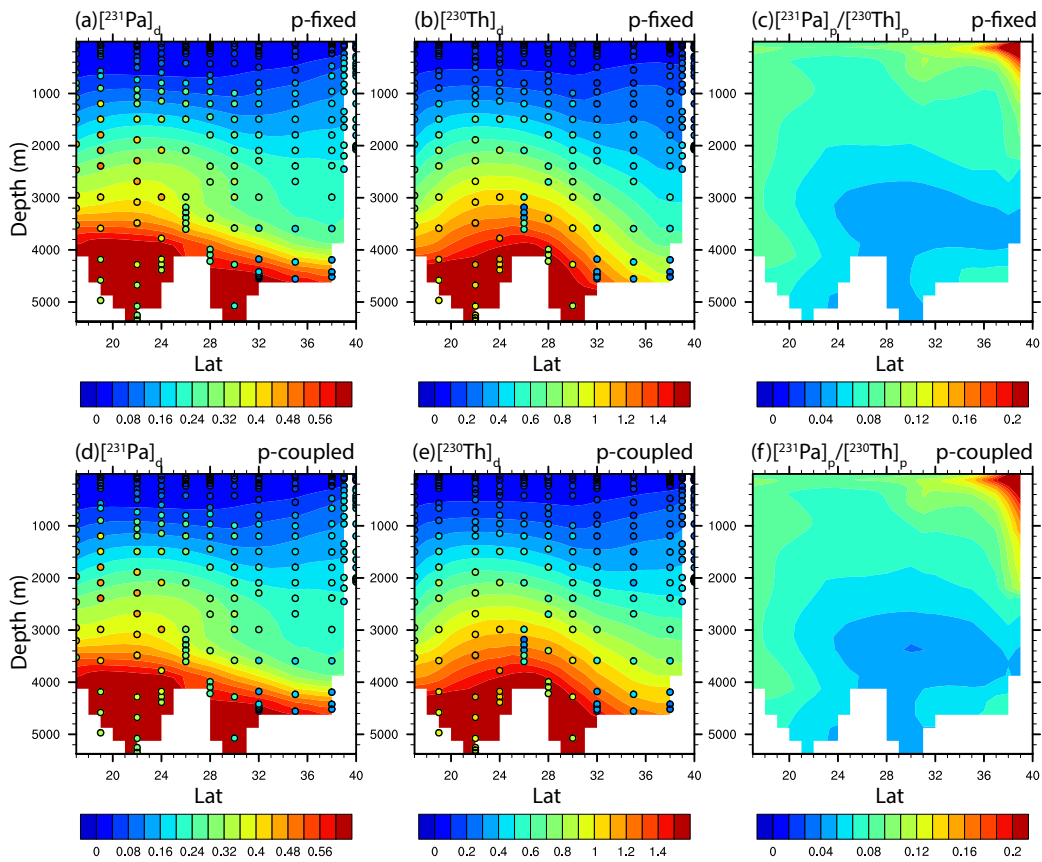
930

931 Figure 3. Dissolved ^{231}Pa, dissolved ^{230}Th and particulate ^{231}Pa/^{230}Th in CTRL along

932 GEOTRACES transect GA03 (Hayes et al., 2015) (the track is indicated in Fig. S4) for

933 both p-fixed and p-coupled ^{231}Pa and ^{230}Th. Observations of dissolved ^{231}Pa and

934 ^{230}Th activity are superimposed using the same colormap.
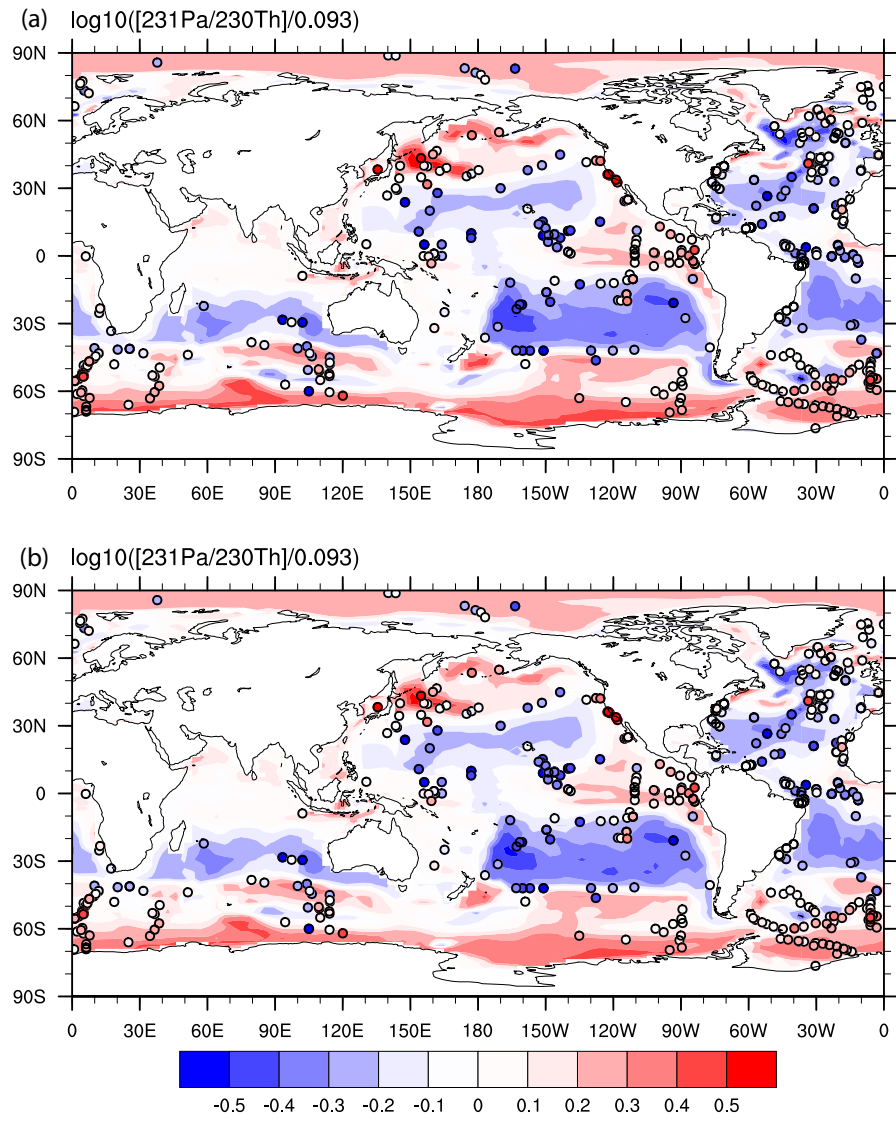
935

936 Figure 4. Sediment ^{231}Pa/^{230}Th activity ratio in CTRL for both p-fixed (a) and p-

937 coupled version (b). Observations are attached as filled cycles using the same color

938 map. The ^{231}Pa/^{230}Th activity ratio is plotted relative to the production ratio of

939 0.093 on a $\log_{10}$ scale.

940

941

942

943
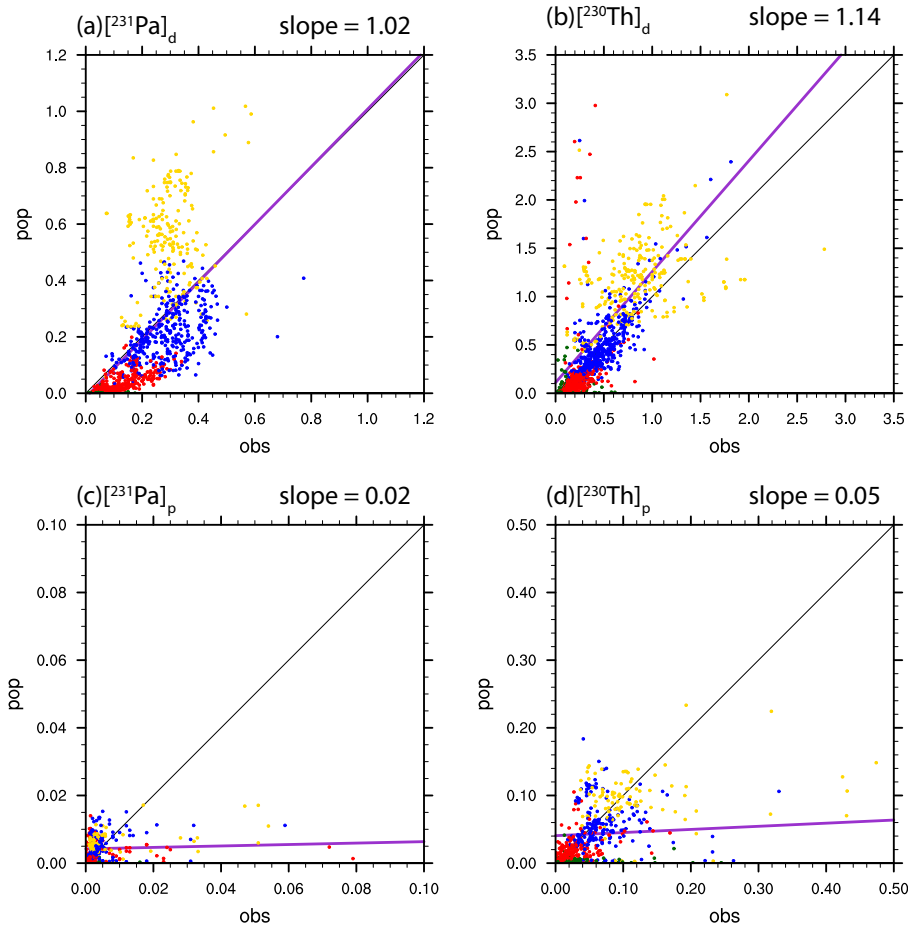
944

945   Figure 5. Scatter plot of global dissolved and particulate ^{231}Pa and ^{230}Th between

946   observation and CTRL (p-fixed) (unit: dpm/m^3). (a) dissolved ^{231}Pa; (b) particulate

947   ^{231}Pa; (c) dissolved ^{230}Th; (d) particulate ^{230}Th. Observations in different depth

948   range are indicated by different colors: green for 0-100m; red for 100m-1000m;

949   blue for 1000m-3000m and yellow for deeper than 3000m. Purple line is the least

950   squared linear regression line and slope is the linear regression coefficient.
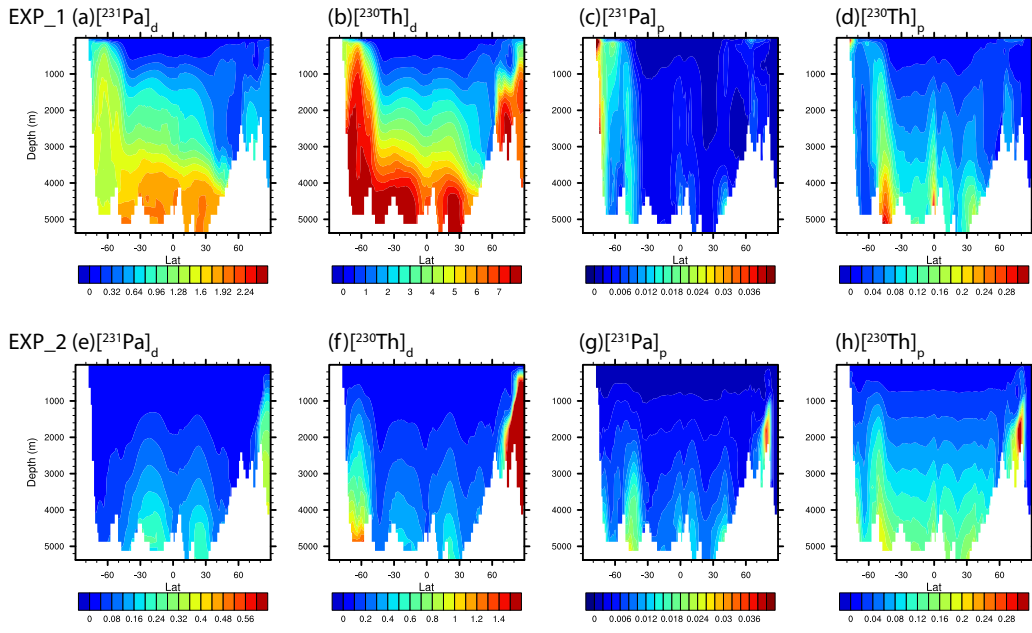
951

952 Figure 6. Atlantic zonal mean dissolved and particulate [231]Pa and [230]Th in EXP_1 and

953 EXP_2 (unit: dpm/m³). EXP_1: (a) dissolved [231]Pa; (b) dissolved [230]Th; (c)

954 particulate [231]Pa; (d) particulate [230]Th. EXP_2: (e) dissolved [231]Pa; (f) dissolved

955 [230]Th; (g) particulate [231]Pa; (h) particulate [230]Th.

956
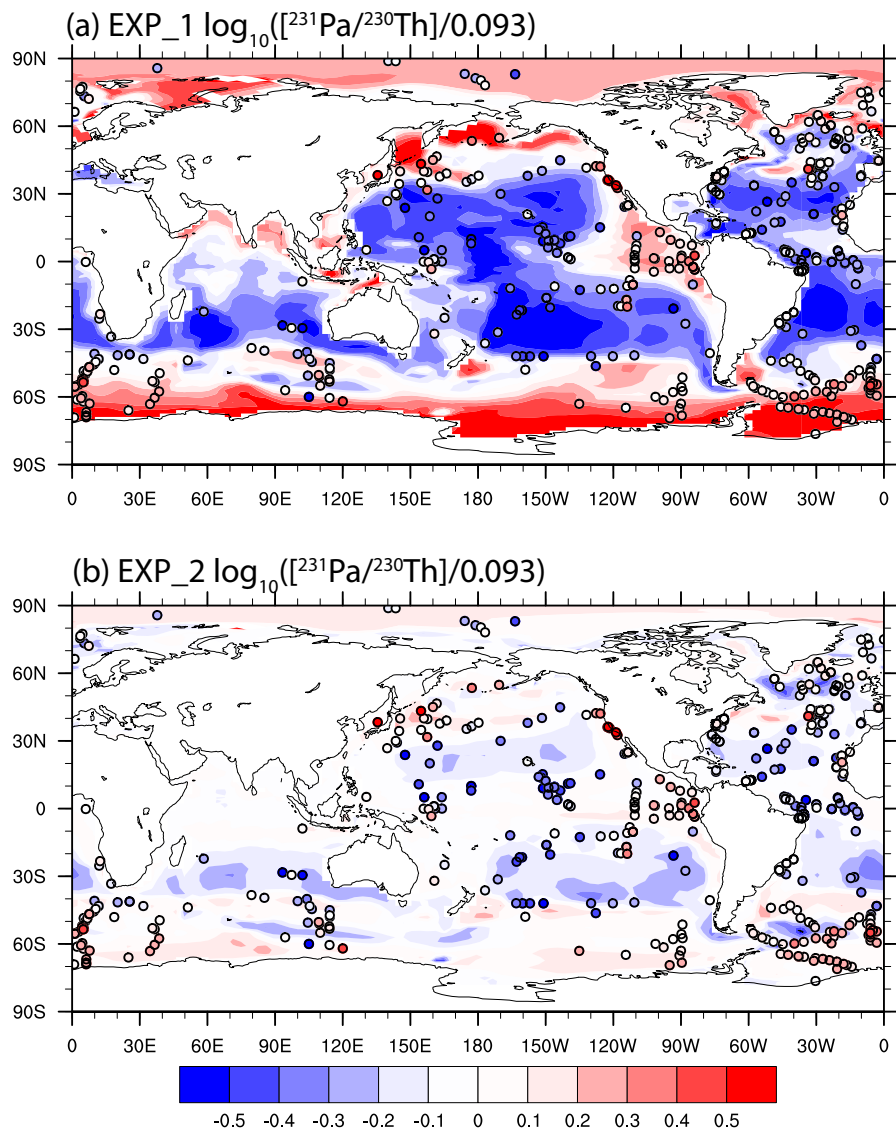
957

958   Figure 7. Sediment ^{231}Pa/^{230}Th activity ratio in EXP_1 (a) and EXP_2 (b).

959   Observations are attached as filled cycles using the same color map. The ^{231}Pa/^{230}Th

960   activity ratio is plotted relative to the production ratio of 0.093 on a $\log_{10}$ scale.

961
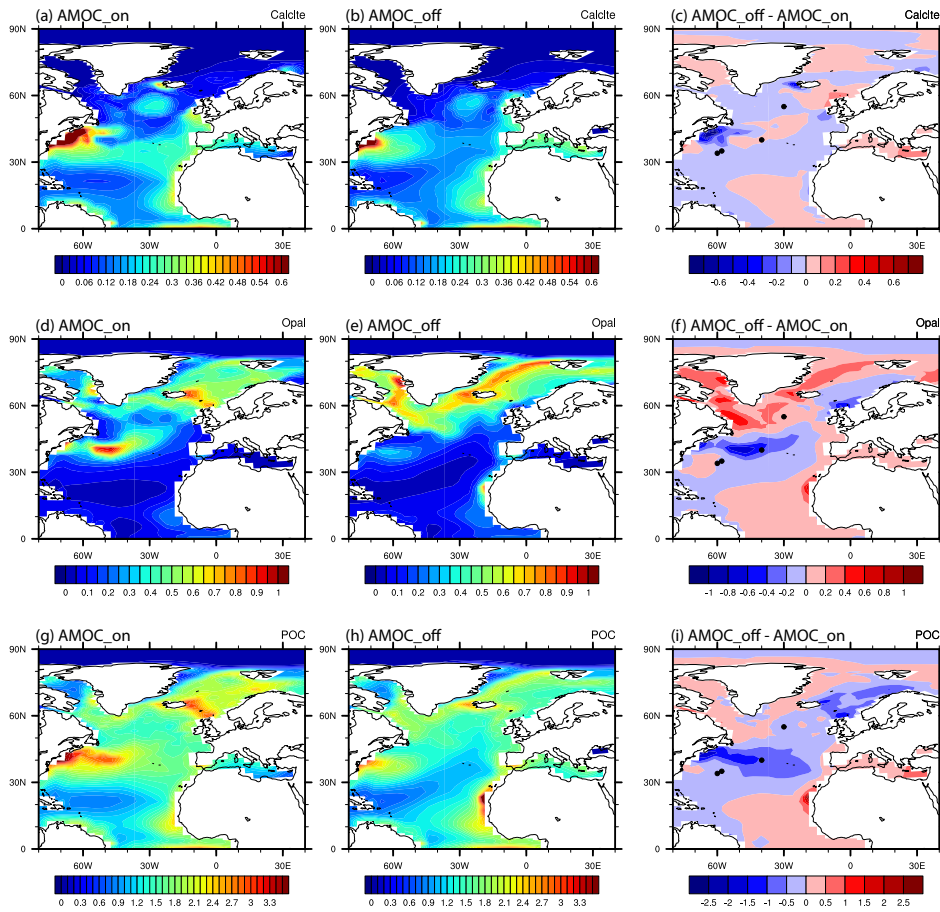
962

963 Figure 8. Comparison of particle fluxes between AMOC_on and AMOC_off. CaCO$_3$ flux

964 at 105m (mol m^{-2} yr^{-1}) during AMOC_on (a), AMOC_off (b) and difference between

965 AMOC_off and AMOC_on. (b) Opal flux at 105m (mol m^{-2} yr^{-1}) during AMOC_on (d),

966 AMOC_off (e) and difference between AMOC_off and AMOC_on (f). POC flux at 105m

967 (mol m^{-2} yr^{-1}) during AMOC_on (g), AMOC_off (h) and difference between AMOC_off

968 and AMOC_on (i).

969

970
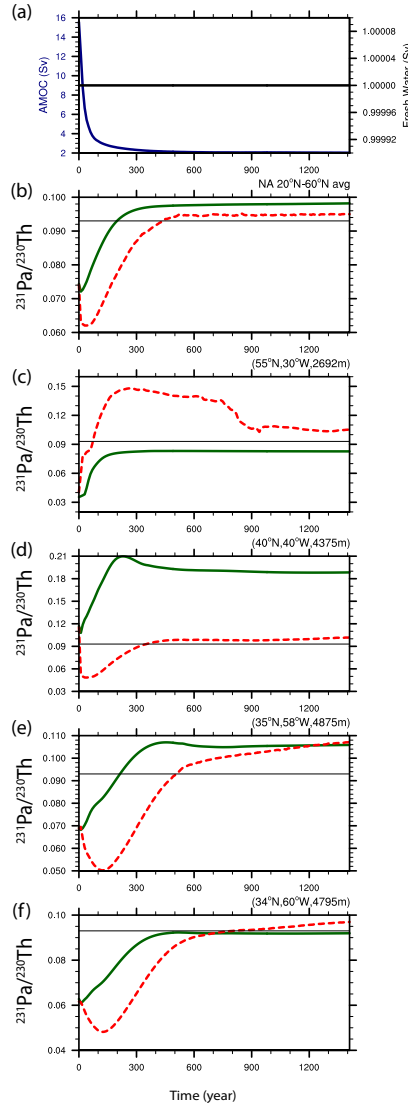
Figure 9. Time evolutions in HOSING. (a) Freshwater forcing (black) and AMOC strength (navy), which is defined as the maximum of the overturning streamfunction below 500m in the North Atlantic. (b) North Atlantic average sediment ^{231}Pa/^{230}Th activity ratio from 20°N to 60°N: p-fixed (green) and p-coupled (red). Production ratio of 0.093 is indicated by a solid black line (similar in c, d, e and f). (c) Sediment ^{231}Pa/^{230}Th activity ratio at (55°N, 30°W). (d) Sediment ^{231}Pa/^{230}Th activity ratio at (40°N, 40°W). (e) Sediment ^{231}Pa/^{230}Th activity ratio at (35°N, 58°W). (f) Sediment ^{231}Pa/^{230}Th activity ratio at (34°N, 60°W). (e) and (f) are near Bermuda Rise. Locations of each site are shown as dots in Fig. 8b.

983
984
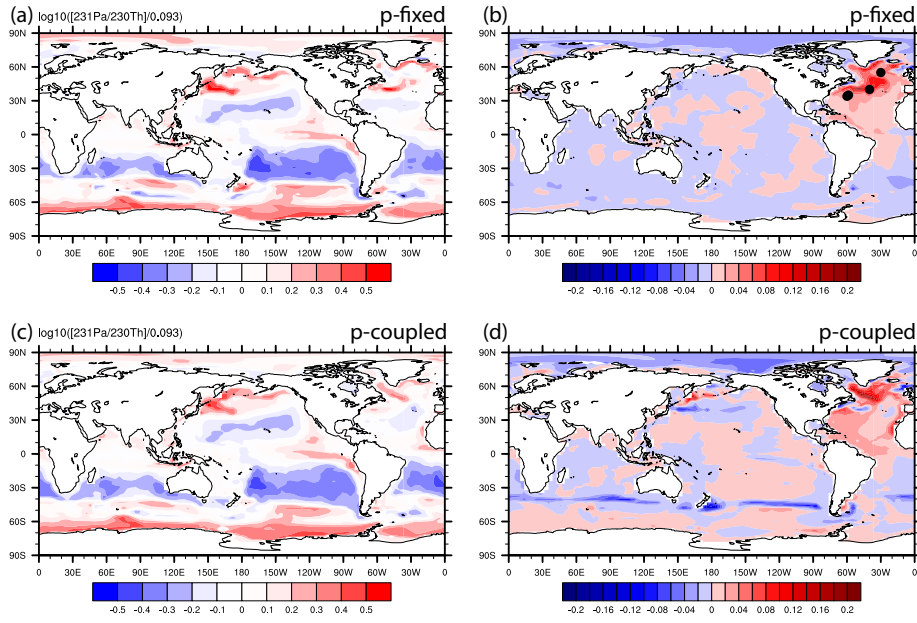
Figure 10. Sediment ^{231}Pa/^{230}Th activity ratio during AMOC off state and the difference between AMOC off and CTRL. (a) P-fixed $\log_{10}([^{231}$Pa/^{230}Th$]/0.093)$ in AMOC_off. (b) Difference of p-fixed sediment ^{231}Pa/^{230}Th activity ratio between AMOC_off and AMOC_on. (c) and (d) are similar to (a) and (b) for p-coupled sediment ^{231}Pa/^{230}Th activity ratio. Black dots in (b) shows the locations of sites in Fig. 9 from North to South.

991
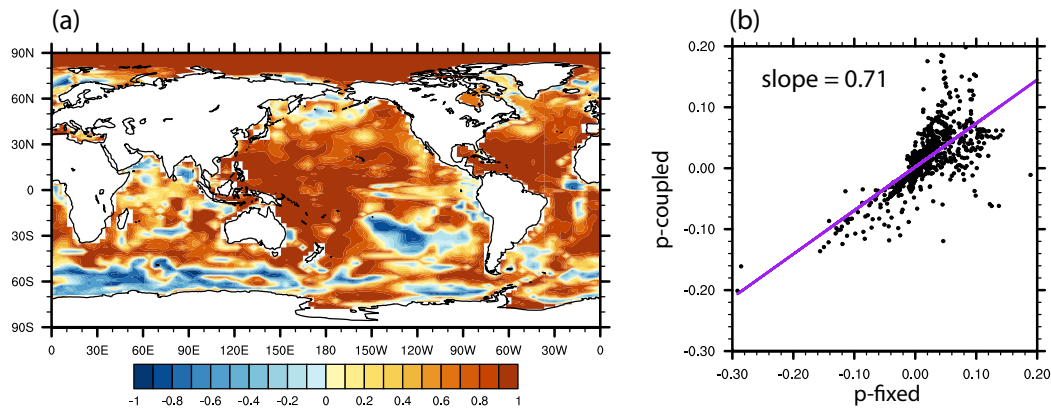
992

993 Figure 11. (a) Correlation of p-fixed and p-coupled evolution of sediment
994 ^{231}Pa/^{230}Th activity ratio in HOSING. (b) Scatter plot of p-fixed and p-coupled
995 sediment ^{231}Pa/^{230}Th activity ratio change from AMOC_on to AMOC_off in the
996 Atlantic and the Southern Ocean (70°W-20°E). Purple line is the least squared linear
997 regression line and slope is the linear regression coefficient.

998
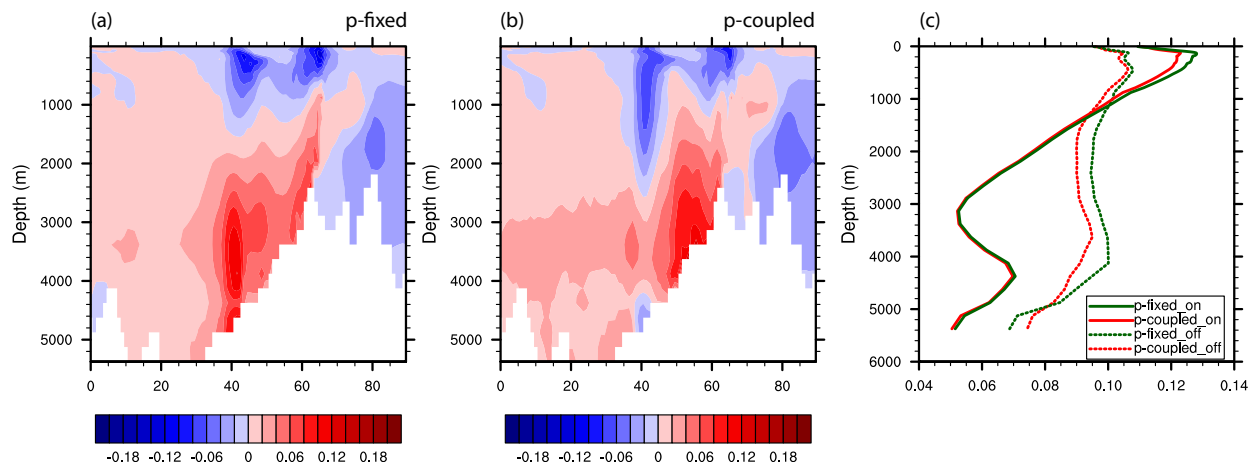
999

1000 Figure 12. Difference of Atlantic zonal mean particulate ^{231}Pa/^{230}Th between
1001 AMOC_off and AMOC_on: (a) p-fixed and (b) p-coupled. (c) North Atlantic (20°N-
1002 60°N) average profile during AMOC_on (solid) and AMOC_off (dash) for p-fixed
1003 (green) and p-coupled (red) particulate ^{231}Pa/^{230}Th.

1004

1005

1006

1007